Cerebral Cortex, April 2018;28: 1439–1457

doi: 10.1093/cercor/bhx352
Advance Access Publication Date: 10 January 2018
Original Article

ORIGINAL ARTICLE

Morphological and Functional Characterization of Non-fast-Spiking GABAergic Interneurons in Layer 4 Microcircuitry of Rat Barrel Cortex

Vishalini Emmenegger[1,2,5,†], Guanxiao Qi[1,†], Haijun Wang[1,2,3] and Dirk Feldmeyer[1,2,4]

[1]Institute of Neuroscience and Medicine, INM-2 and INM-10, Research Centre Jülich, D-52425 Jülich, Germany, [2]Department of Psychiatry, Psychotherapy and Psychosomatics, RWTH Aachen University, D-52074 Aachen, Germany, [3]School of Electronic Engineering, Nanjing Xiaozhuang University, Nanjing 211171, P.R. China, [4]Jülich Aachen Research Alliance, Translational Brain Medicine (JARA Brain), D-52074 Aachen, Germany and [5]Current address: Department of Biosystems Sciences and Engineering, Bio Engineering Lab, ETH Zürich, 4058 Basel, Switzerland

Address correspondence to Dirk Feldmeyer, Institute of Neuroscience and Medicine (INM-2), Research Centre Jülich, D-52425 Jülich, Germany. Email: d.feldmeyer@fz-juelich.de

[†]These authors contributed equally to this work.

Abstract

GABAergic interneurons are notorious for their heterogeneity, despite constituting a small fraction of the neuronal population in the neocortex. Classification of interneurons is crucial for understanding their widespread cortical functions as they provide a complex and dynamic network, balancing excitation and inhibition. Here, we investigated different types of non-fast-spiking (nFS) interneurons in Layer 4 (L4) of rat barrel cortex using whole-cell patch-clamp recordings with biocytin-filling. Based on a quantitative analysis on a combination of morphological and electrophysiological parameters, we identified 5 distinct types of L4 nFS interneurons: 1) *trans-columnar projecting interneurons*, 2) *locally projecting non-Martinotti-like interneurons*, 3) *supra-granular projecting Martinotti-like interneurons*, 4) *intra-columnar projecting VIP-like interneurons*, *and* 5) *locally projecting neurogliaform-like interneurons*. Trans-columnar projecting interneurons are one of the most striking interneuron types, which have not been described so far in Layer 4. They feature extensive axonal collateralization not only in their home barrel but also in adjacent barrels. Furthermore, we identified that most of the L4 nFS interneurons express somatostatin, while few are positive for the transcription factor Prox1. The morphological and electrophysiological characterization of different L4 nFS interneuron types presented here provides insights into their synaptic connectivity and functional role in cortical information processing.

Key words: barrel cortex, GABAergic interneuron, Layer 4, non-fast spiking

Introduction

GABAergic inhibitory interneurons play an important role in providing balanced cortical excitation, synchronized activity, suppressing run-away excitation, and in maintaining neuronal oscillatory networks (McBain and Fisahn 2001; Markram et al. 2004; Burkhalter 2008; Klausberger and Somogyi 2008). Alterations in these functional characteristics have been related to several neurological and psychiatric disorders such as autism, epilepsy, schizophrenia, Tourette syndrome and chronic neuropathic pain (Kalanithi et al. 2005; Tabuchi et al. 2007; Gonzalez-Burgos et al. 2015; Jiang et al. 2016; Cichon et al. 2017).

Inhibitory interneurons are highly diverse with respect to their molecular, morphological, electrophysiological and synaptic properties. Such diversity suggests that different groups of interneurons fulfill distinct functional roles in the neuronal network and that the mechanism of synaptic inhibition is neuron-specific (Burkhalter 2008). Therefore, it is of paramount importance to identify the different interneuron types in the neuronal microcircuitry. Ideally, that would take all interneuron characteristics such as their genetic make-up, structural and electrical properties, action potential (AP) firing behavior, synaptic connectivity and developmental profile into account. Such approaches have been undertaken to some extent and have become increasingly more refined in recent years (Gupta et al. 2000; Ascoli et al. 2008; Burkhalter 2008; DeFelipe et al. 2013; Kepecs and Fishell 2014; Lerner et al. 2016; Paul et al. 2017; Zeng and Sanes 2017). Nevertheless, interneuron classification is still challenging and suffers from a lack of consensus about classification parameters and often substantial differences in terminology (Hamilton et al. 2017).

In this study, we attempted to work on a small subset of neocortical interneurons in order to assess and quantitatively analyse their morphological and electrophysiological diversity. Layer 4 (L4) of sensory cortices shows the highest density of thalamocortical afferents and thus serves as the major intracortical target structure for sensory input-related synaptic signals. From there, L4 excitatory neurons serve in the distribution of these signals within and beyond the sensory cortex. In these processes L4 inhibitory interneurons are likely to play important roles in regulating intracortical excitatory signal flow as well as shaping its "temporal" characteristics.

In the barrel cortex, a single barrel in cortical Layer 4 is known to process the information of one defined whisker (Woolsey and van der Loos 1970). In the rat, a single barrel contains about 4000 neurons, of which only 8.1% are interneurons, the lowest fraction in any layer of the somatosensory cortex (Meyer et al. 2011).

It has been proposed that 3 major groups of neocortical GABAergic interneurons exist, i.e., those expressing either parvalbumin (PV; and show high-frequency action potential firing) or the neuropeptide somatostatin (SOM) or the ionotropic serotonin receptor (5-HT_{3a}R). Of the latter, 40% have been shown to co-express the vasoactive-intestinal peptide (VIP) (Lee et al. 2010; Rudy et al. 2011; Tremblay et al. 2016) but recent studies using large-scale RNA-sequencing suggest that the diversity is much larger (Zeisel et al. 2015; Cadwell et al. 2016; Fuzik et al. 2016; Lake et al. 2016; Tasic et al. 2016; Johnson and Walsh 2017; Paul et al. 2017).

In Layer 4, the majority (~60–80%) are PV-positive, fast-spiking (FS) interneurons, of which a L4 basket cell with a very dense axonal plexus and a high synaptic connectivity (Koelbl et al. 2015) is the most common although other FS interneuron types exist. The remaining L4 interneuron types, the so-called non-fast-spiking (nFS) interneurons, were described in previous studies as low threshold spiking (LTS) and/or regular spiking non-pyramidal cells (RSNP) in Layer 4 of rodent barrel cortex (Gibson et al. 1999; Porter et al. 2001; Sun et al. 2006). However, to date, no in-depth morphological characterization of these L4 nFS interneurons in rodent barrel cortex or any other sensory cortical area exists. The number of these L4 nFS interneurons amounts to no more than 130 interneurons per cortical barrel.

In this study, the focus was on the examination of the electrophysiological and morphological parameters. These allow a rigorous quantification on the basis of which robust and reliable statistical tests can be performed. Here, we were able to quantitatively characterize different morphological classes of nFS interneurons by using unsupervised cluster analysis based on the axonal and dendritic projection patterns; this resulted in 4 distinct nFS clusters, showing trans-columnar, local, supragranular, and intra-columnar projections. Among others, identification of trans-columnar projecting interneurons from one barrel to neighboring barrels in Layer 4 is a key finding, and we believe that this novel interneuron type could play an important role in early lateral or surround inhibition. Following the morphological identification of nFS interneurons, we analyzed their intrinsic properties, which resulted in the characterization of 3 electrophysiological clusters, differing mainly in their adaptation properties. The combination of morphological and electrophysiological properties provided clusters showing partial correlation, and resulted in a better separation of clusters. The molecular identification of L4 nFS interneurons revealed that 70% are SOM-positive and 15% are Prox1-positive comprising neurogliaform cell (NGFC)-like and VIP-like interneurons. The heterogeneity of L4 nFS interneurons with respect to their morphological, electrophysiological, and molecular properties could serve different functional roles in the intra- and inter-columnar processing of sensory signals.

Materials and Methods

Slice Preparation

All experiments were performed in accordance with the guidelines of the Federation of European Laboratory Animal Science Association (FELASA), with the EU Directive 2010/63/EU, and with the German animal welfare act, and were approved by the Northrhine-Westphalian Landesamt für Natur-, Natur- und Verbraucherschutz (LANUV). The animals used for this study were Wistar rats (Charles River, either sex) aged 17–21 postnatal days (P17–21). The experimental procedures were adopted from Agmon and Connors with minor modifications (Agmon and Connors 1991). Rats were deeply anaesthetized with isoflurane and decapitated. The brain was removed and transferred to an ice-cold (~4 °C) preparation solution with a high magnesium and low calcium concentration (i.e., 4 mM $MgCl_2$ and 1 mM $CaCl_2$) to minimize spontaneous synaptic activity. The solution was bubbled continuously with carbogen gas (95% O_2 and 5% CO_2) to maintain adequate oxygenation and a physiological pH level. About 350 μm thick oblique coronal slices of the somatosensory cortex were cut at an angle of 45° to the midline at a high vibration frequency and at a slow speed (Chmielowska et al. 1989; Feldmeyer et al. 1999; L). The slices were incubated for ~1 h at room temperature (21–24 °C) in the slicing solution and subsequently placed in the recording chamber. Neurons were visualized under an upright microscope, fitted with 4×/0.13 numerical aperture (NA) and 40× water immersion/0.80 NA objectives (Olympus Deutschland GmbH, Hamburg, Germany). Under bright-field illumination at low magnification, barrels in Layer 4 can be

seen as light hollow barrel-like structures with narrow dark stripes in between (Feldmeyer et al. 1999). Even though barrel structures were present in 6–8 slices, a continuous band of barrels was visible only in the last 2–3 slices (located 3.5–3.6 mm caudal to bregma). Under infrared differential inference contrast (IR-DIC) microscopy, individual L4 neurons were visualized at 40× magnification (Dodt and Zieglgänsberger 1990; Stuart et al. 1993).

During whole-cell voltage recordings, slices were continuously perfused (perfusion speed ~5 ml/min) with an artificial cerebrospinal fluid (ACSF) containing (in mM): 125 NaCl, 25 D-glucose, 25 $NaHCO_3$, 2.5 KCl, 2 $CaCl_2$, 1.25 NaH_2PO_4 and 1 $MgCl_2$, bubbled with carbogen gas, and maintained at a temperature of 31–33 °C. Patch pipettes were pulled from thick-wall borosilicate glass capillaries (outer diameter 2.0 mm; inner diameter 1.0 mm) and filled with an internal solution containing (in mM): 135 K-gluconate, 4 KCl, 10 HEPES, 10 phosphocreatine, 4 Mg-ATP, and 0.3 GTP (pH 7.4, 290–300 mOsm) supplemented with 5 mg/ml biocytin (13.4 mM) to obtain permanent staining to allow morphological analyses after the electrophysiological recordings.

Electrophysiological Recordings

Whole-cell patch-clamp recordings were performed using patch pipettes of 5–7 MΩ resistance. Neurons in Layer 4 of the barrel cortex that were located at least 50 µm below the slice surface were selected randomly and independent of their location in the barrel. The cell bodies of L4 nFS interneurons resembled those of other L4 neurons; some were large and ovoid-shaped and thus similar to those of L4 FS interneurons, while others resembled the round to polygonal cell bodies of L4 spiny neurons (Feldmeyer et al., 1999; Koelbl et al., 2015). We used the intrinsic firing patterns recorded in the current clamp mode to reliably differentiate nFS interneurons from other neuron types.

The resting membrane potential (V_{rest}) was measured immediately after establishing the whole-cell configuration. Bridge balance and capacitance neutralization were adjusted. A series of 1 s-long current steps, ranging from −100 pA to +500 pA in 10–25 pA stepped depolarizations was injected at 1 s intervals. Membrane potentials were not corrected for a junction potential, which was calculated to be −15.8 mV (Barry and Lynch 1991; Barry 1994). The recordings were made using an EPC10 amplifier (HEKA, Lambrecht, Germany). Data were filtered at 2.9 kHz and sampled at 10 kHz using Patch master software (HEKA), and later analyzed off-line using Igor Pro software (Wavemetrics).

Histological Procedures

After the electrophysiological recordings, slices containing biocytin-filled neurons were processed using a protocol described previously (Marx et al. 2012; Radnikow et al. 2012). The slices were fixed in 4% PFA (12.9 mM) in 100 mM phosphate buffer solution (PBS) for at least 24 h at 4 °C. To block any endogenous peroxidase activity, the slices were treated with 3% H_2O_2 (29.4 mM) solution in PBS for about 20 min. The slices were rinsed repeatedly using 100 mM PBS and subsequently incubated at room temperature in 1% avidin-biotinylated horseradish peroxidase (Vector ABC staining kit, Vector Lab. Inc.) containing 0.1% Triton X-100 for 1 h. This was followed by chromogenic reaction by adding 0.5 mg/ml (13.4 mM) 3,3-diaminobenzidine (DAB; Sigma-Aldrich, USA) until the biocytin-filled neurons with distinct axonal and dendritic branches were clearly visible. The slices were rinsed again with 100 mM PBS, then dehydrated slowly for 2–4 h with increasing ethanol concentrations and finally in xylene (see Marx et al. 2012 for details). The slices were then mounted on gelatinized slides and embedded using Eukitt medium (Otto Kindler GmbH).

Immunohistochemical Staining

For the identification of molecular markers expressed by GABAergic interneurons, we prepared 100 µm thin brain slices using a vibratome. The brain slices were immediately fixed with 4% PFA in 100 mM PBS for at least 24 h at 4 °C. For some antibodies (anti-VIP), we followed a shorter fixation time of 2 h. The slices were then permeabilized in 0.5% Triton X-100 in 100 mM PBS with 1% milk powder for 1 h at room temperature. Primary and secondary antibodies for PV, SOM, 5-HT_{3a}R, Prox1 and VIP (listed in Supplementary Table 1) were diluted in a permeabilization solution containing 0.5% Triton X-100 and 100 mM PBS. Subsequently, the slices were incubated overnight in a solution containing the respective primary antibody at 4 °C and then rinsed thoroughly with 100 mM PBS. The slices were then treated with the secondary antibodies for 2–3 h at room temperature in the dark. Controls were also performed in the absence of primary and secondary antibodies. After being rinsed in 100 mM PBS for several times, the slices were embedded in Moviol and visualized by transmitted light fluorescence microscopy using an upright microscope equipped with fluorescence optics. The fluorescence images were taken using the Olympus CellSens platform.

In a subset of experiments, we tried to identify the expression of molecular markers in single L4 nFS interneurons in brain slices to investigate a possible correlation with the electrophysiological and morphological properties. To this end, we added Alexa Fluor® 594 biocytin salt (1:500, Invitrogen, Darmstadt, Germany) to the internal solution (composition as described above) to identify the patched neurons in the post hoc antibody labeling methods. After recording, the slices were fixed in 4% PFA in 100 mM PBS for 2 to 24 h at 4 °C; for antibody labeling, we followed the procedure as described above. The position of the biocytin-stained neuron was visualized by the conjugated Alexa dye, so that the expression of a specific molecular marker could be tested in identified individual neurons. After acquiring fluorescent images, the slices were incubated in 100 mM PBS overnight and subsequently processed for morphological analyses (see above).

Morphological 3D Reconstructions

Biocytin-labeled neurons in Layer 4 were morphologically reconstructed using Neurolucida® software (MicroBrightField, Williston, VT, USA) on an upright microscope equipped with a motorized stage. An oil-immersion objective at a magnification of 100x was used. Along with the neuronal reconstructions, cytoarchitectonic features such as the barrels and layers were also labeled under the low magnification objective. Eukitt embedding reduced fading of cytoarchitectonic features and enhanced the contrast between layers (Marx et al. 2012). To provide further enhancement, the condenser aperture diaphragm was closed, which facilitated displaying the density and the size of soma across different layers. The borders between Layers 2/3, Layer 4, and Layer 5a were differentiated based on the appearance of cortical barrels, whereas Layers 5 and 6 were distinguished by the size of the pyramidal cell soma. Furthermore, the position of soma, barrels and layers were confirmed by correlating with the DIC images during the recording. After the reconstruction, the images were rotated such that the pial surface was in the horizontal plane. The tissue shrinkage was corrected for using shrinkage correction factors of

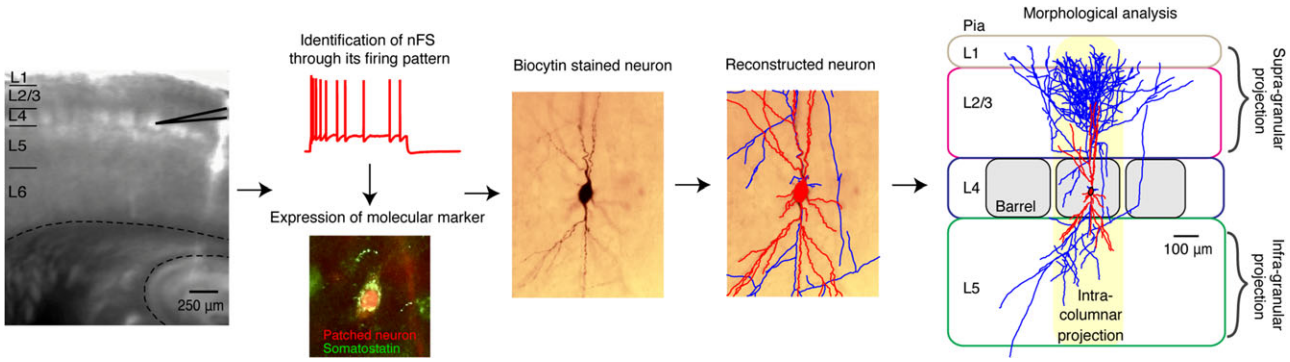

Figure 1. Schematic representation of experimental approach. Individual neurons in Layer 4 of rat barrel cortex were recorded using whole-cell patch-clamp technique and filled with biocytin. nFS interneurons were identified by their firing patterns. In a subset of experiments, biocytin was conjugated to Alexa dye, to identify the expression of specific molecular marker of the patched neuron using immunofluoresence microscopy. Later biocytin labeling was histochemically processed to obtain a permanent stain of the neurons. For a quantitative analysis, the 3D morphology of patched neurons was reconstructed using Neurolucida software. The axon is labeled in blue; soma and dendrites in red. Layers, barrels (gray) and cortical column (yellow) were demarcated for further quantitative analysis. Percentage of axonal projections within home barrel, adjacent barrel, supra-granular layers, infra-granular layers, intra-column were used to classify the nFS interneuron types.

1.1 in the *x*–*y* direction and 2.1 in the *z* direction (Marx et al. 2012). An analysis of 3D reconstructed neurons was performed using the Neuroexplorer® software (MicroBrightField, Williston, VT, USA; see Fig. 1).

Data Analysis

Membrane and Spike Properties

The resting membrane potential (V_{rest}) and the series resistance was measured immediately after establishing the whole-cell configuration. Only neurons with a stable V_{rest} between −55 and −75 mV and a series resistance of less than 40 MΩ were included for the data analysis to guarantee a high recording quality. The recorded data were analyzed using custom-written macros in Igor Pro 6 (WaveMetrics).

Passive membrane properties such as the input resistance R_{in}, membrane time constant τ_m, voltage sag, and rheobase were determined. AP threshold, amplitude, half-width, AHP amplitude were measured for the first spike elicited by a rheobase current step. AP amplitude accommodation and frequency adaptation were measured for the current step that elicited close to 10 APs. See Table 1 for descriptions of all electrophysiological parameters.

Morphological Properties

For a reliable quantitative analysis, neurons were either not reconstructed at all or excluded from the data analysis based on the following criteria:

1. If the neurons showed a weak dye labeling or high background staining (Supplementary Fig. 1*A*).
2. If the primary branch of an axon was truncated before it started to bifurcate (Supplementary Fig. 1*B*).
3. Another important factor for determining the completeness of the neuronal morphology is the angle at which the brain slice is cut. For this, we identified dendritic and axonal endings that showed clear signs of truncation, such as a bleb at its ending (so-called incomplete endings) or a truncation at the slice surface (so-called high endings). The percentage of truncations was calculated as the ratio of the combined number of high and incomplete endings to the number of total endings. Only those L4 nFS interneurons were included in the analysis for which the incomplete/high axonal endings were ≤15% of the total number of endings (Supplementary Fig. 1*C*).

Analysis of 3D reconstructed interneurons was performed using the Neuroexplorer software. Morphological properties of interneurons such as the length and the distribution of axons and dendrites across different layers and adjacent barrels were analyzed (Helmstaedter et al. 2009b). The description of all the morphological parameters is listed in Table 1.

Principal Component Analysis

The dataset of L4 nFS interneurons was represented in the form of a matrix in which rows correspond to individual interneurons and columns to variables. Since the parameters often had different units, especially the electrophysiological parameters, they were standardized using z-score in order to make the distributions numerically comparable. Principal component analysis (PCA) was then used to analyze the interdependence between variables and to reduce the dimensionality of the dataset while preserving maximum variability. PCA reduces the redundancy of the dataset by eliminating correlated variables and produces linear combinations of the original variables to generate new axes; the latter are also known as principal components (PCs) that are orthogonal and, therefore, uncorrelated.

To determine the number of PCs to retain for cluster analysis, we used Kaiser's rule, which is one of the most widely used criteria (Fabrigar et al. 1999). Kaiser's rule is an objective way to determine the number of clusters by leaving all components with eigenvalues less than 1. Since the dataset is standardized, the variables have an eigenvalue of 1, and hence, PCs with an eigenvalue greater than 1 describe more of the data's variance than the original variable.

Unsupervised Hierarchical Cluster Analysis

Quantitative classification was performed using unsupervised hierarchical cluster analysis (CA) that determines how different, or how similar, two neurons are. CA was performed on the dataset in PC space where the linkage distance was calculated using Euclidean distances. Ward's minimum variance method was used for combining clusters at each stage, which minimizes the total within-cluster variance (Ward 1963). To

Table 1 List of morphological and electrophysiological parameters used for data analysis

	Description
Morphological parameter	
Percentage of axon and dendrites in home barrel (%)	Fraction of axonal and dendritic path length within the home barrel in Layer 4 to the total axonal and dendritic length
Percentage of axon and dendrites in adjacent barrel (%)	Fraction of axonal and dendritic path length in the adjacent barrels to the total axonal and dendritic length
Percentage of axon and dendrites in Layer 4 (%)	Fraction of axonal and dendritic path length within the home layer to the total axonal and dendritic length
Percentage of axon and dendrites in supra-granular layers (%)	Fraction of axonal and dendritic path length in Layer 1 and Layer 2/3 to the total axonal and dendritic length
Percentage of axon and dendrites in infra-granular layers (%)	Fraction of axonal and dendritic path length in Layer 5 and Layer 6 to the total axonal and dendritic length
Percentage of axon and dendrites in intra-column (%)	Fraction of axonal and dendritic path length within the home column extending to all layers and including half of the adjacent septa on both sides to the total axonal and dendritic length
Electrophysiological parameters	
Resting membrane potential, V_{rest} (mV)	Stable membrane potential with no current injection, soon after the seal was broken
Input resistance, R_{in} (MΩ)	Slope of the linear fit between −60 to −70 mV of the current–voltage (I–V) response curve
Voltage sag (%)	Difference between the most hyperpolarized voltage and the steady-state voltage deflection, divided by the steady-state deflection
Membrane time constant, τ_m (ms)	Mono-exponential fit of the hyperpolarising voltage response after a current step of −50 pA
Rheobase (pA)	Minimal current that elicited the first spike
AP threshold (mV)	The point of start of acceleration of the membrane potential using the second derivative of the membrane potential (d2V/dt2)
AP amplitude (mV)	Difference in voltage from AP threshold to the peak during depolarization
AP half-width (ms)	Time difference between rising phase and decaying phase of the AP at half-maximum amplitude
AP latency (ms)	Time required for the onset of first AP in rheobase current stimulus
AHP amplitude (mV)	Difference in voltage from AP threshold to maximum deflection of the repolarization
AP amplitude accommodation (mV)	Difference between the average of the first 3 APs and the last 3 APs
Average of inter-spike interval, ISI (ms)	Average time taken between individual spikes
CV of ISI (ms)	Coefficient of variance of ISIs
Frequency adaptation ISI_1/ISI_9	Ratio of the first ISI to the last ISI
Frequency adaptation ISI_{min}/ISI_{max}	Ratio of the minimum ISI to the maximum ISI
Frequency-current slope (Hz/pA)	Slope of the linear fit of the frequency-current response curve between 0 and 300 pA
Maximum firing frequency (Hz)	Highest firing frequency neurons could attain during 1 s of current injection

visualize the distance at which clusters are combined, a dendrogram was constructed where the vertical lines show joined clusters.

Determining the Optimal Number of Clusters

Silhouette analysis measures the quality of clustering by calculating the separation between the resulting clusters (Rousseeuw 1987). The silhouette plot shows a measure of proximity of neighboring clusters within a dataset. This measure ranges from −1 to 1. A silhouette width close to 1 means that the dataset in one cluster is highly separated from the neighboring clusters. A width of −1 indicates that the dataset might be wrongly assigned. The average silhouette width represents the overall strength of all clusters. The larger the average silhouette width, the better the clustering. In order to determine the final number of clusters in the dendrogram, the average silhouette width for all possible clusters was plotted. The number of clusters yielding the maximum average silhouette width was chosen as it indicates the optimal separation of clusters.

K-means Clustering

K-means is an alternative clustering method, where the number of clusters K is user-specified; it is therefore a supervised clustering approach (Forgy 1965; MacQueen 1967). In this study, K-means clustering was performed with K equal to the number of clusters with the highest average silhouette width. The K-means method first randomly identifies initial centroid positions, also known as seeds, for each cluster. Each dataset is grouped to the nearest centroid to form a set of temporary clusters. The mean point of the temporary cluster is then assigned as the new centroid, the data points are rearranged, and the process continues until there is no change in the clusters. K-means was repeated 100 times with random initial centroid positions to ensure convergence to the global optimum.

Axonal and Dendritic Density Maps

The 3D density maps of axonal and dendritic length were obtained using computerized 3D reconstructions, where the length of the axonal and dendritic tree per unit volume of $50 \times 50 \times 50\,\mu m^3$ was calculated (Lubke et al. 2003; Narayanan et al. 2015). The soma center of each neuron was given the co-ordinates of X, Y, Z = (0, 0, 0), and the relative coordinate of the beginning and endpoint of each segment in the tracing were obtained using the segment point analysis in Neuroexplorer®. Further steps were carried out in Matlab (MathWorks) using a custom-written algorithm. The 3D axonal and dendritic density maps were calculated for each reconstructed interneuron from a single cluster. These were then averaged to obtain the 3D density map for this cluster.

Individual density maps were aligned with respect to the soma center. The averaged density map for each cluster was smoothed using the 3D smooth function in Matlab with a Gaussian kernel (s.d. = 50 μm). Isosurfaces at the 80-percentile were calculated for the smoothed density maps. Finally, axonal and dendritic density maps were visualized in blue and red, respectively.

Statistical Analysis

Data are represented as mean ± standard deviation (SD). In order to determine the contribution of different variables for distinguishing the different clusters, one-way ANOVA was used followed by a post hoc Tukey's HSD test where clusters were compared for significant differences. Statistically significant differences among the clusters (see Supplementary Tables 3 and 4 and Figs 2*E* and 3*E*) are reflected in a high contribution of parameters in the PC space (Supplementary Tables 3 and 4).

Results

In order to characterize the different L4 nFS interneurons, we recorded 105 nFS interneurons using whole-cell patch-clamp recordings and simultaneous biocytin-filling for post hoc morphological reconstruction of the recorded neurons using Neurolucida software (Fig. 1). To this end, we distinguished nFS interneurons from the FS interneurons using 3 electrophysiological parameters, such as the AP half-width, the AHP amplitude and the maximum firing frequency (Fig. 3*A*, inset). In a subset of experiments, we performed antibody labeling of the recorded nFS interneurons to identify the marker expression of the patched neurons. Most of the nFS interneurons were found to be SOM-positive. We employed quantitative classification methods based on morphological and electrophysiological properties that yielded reliable identification of different subtypes in the L4 microcircuitry of rat barrel cortex.

Morphological Classification of nFS Interneurons

After processing for biocytin, 59 nFS interneurons with low background staining were reconstructed using Neurolucida® software. Following the criteria as outlined in the Materials and Methods section, we included 48 high-quality complete 3D morphological reconstructions for the final data analysis. For the quantitative classification of nFS interneurons, an unsupervised hierarchical CA was performed based on their axonal and dendritic projection patterns (see Table 1, Supplementary Tables 2 and 3). The first 3 PCs with eigenvalues greater than 1 were retained for CA; they showed a cumulative variance of about 80%. The percentage of contribution of the parameters is listed in Supplementary Table 3. CA revealed 4 distinct morphological clusters (MCs) of L4 nFS interneurons, as shown in the dendrogram in Fig. 2*A* (labeled magenta, cyan, green, and orange).

The 4 clusters were distinct in both their axonal and dendritic projection patterns (Fig. 2*C*,*D*). Morphological cluster 1 (MC1) interneurons showed prominent axonal and dendritic projections to neighboring barrels and were therefore designated as trans-columnar or lateral projection neurons. The axon and dendrites of cluster 2 (MC2) interneurons were largely confined to the home barrel and were therefore named local projection neurons. Cluster 3 (MC3) interneurons displayed a distinct axonal projection pattern, with extensive branching in supra-granular layers, and only few collaterals in the home layer. Cluster 4 (MC4) showed a bipolar dendritic domain and sparse axonal projections to the supra- and infra-granular layers, which were almost exclusively confined to the home column; these features were similar to those of VIP+ interneurons (Porter et al. 1998; Pronneke et al. 2015). Of the 48 L4 nFS interneurons that were classified into 4 main clusters, 8 interneurons belonged to MC1 (17%), 28 interneurons to MC2 (58%), 7 interneurons to MC3 (15%), and 5 interneurons to MC4 (10%) (Fig. 2*B*). Representative interneuron morphologies and density plots for each cluster are shown in Fig. 2*C*,*D*; individual reconstructions of all 48 interneurons are given in Supplementary Fig. 2.

In order to assess the reliability of the cluster assignment obtained by Ward's method, we performed K-means clustering with the predefined number of clusters obtained from the average silhouette width showing the largest value. We found that the dataset in each cluster was generally the same for both the K-means and the hierarchical CA with few misalignments (Supplementary Table 3).

Morphological Cluster 1: Trans-columnar Projecting Neurons

The first group of interneurons, i.e., MC1 interneurons, consisted of 8 interneurons and thus constituted 17% of the nFS interneuron population. The main property of MC1 interneurons was the significant projection to adjacent barrels. This is a novel feature that has not yet been described for L4 interneurons (Fig 2*D*,*E*, Supplementary Video 1); MC1 interneurons also showed a dense and complex axonal arborization; the average total axonal length was 45 ± 12 mm. One of the trans-columnar projecting neurons displayed an exceptionally long axon of around 60 mm. Dendrites had an average total length of 5.8 ± 2.0 mm.

Of all axonal projections, 69.1 ± 10.6% were within the home barrel column, indicating that a significant fraction was outside the column ($P < 0.001$ between all clusters, Table 2). Almost half of the trans-columnar projections (16.4 ± 5.0%) innervated adjacent barrels. In 63% of cases, axons ascended and sent several collaterals to Layer 2/3, and in 37% of cases, the axons terminated in Layer 1 with horizontally projecting collaterals. Only few axon collaterals were found in Layer 5 (8.7 ± 5.0%) and none in Layer 6.

Notably, dendrites followed the projection patterns of the axons (Fig. 2*D*), with a significant proportion (6.1 ± 8.2%) innervating adjacent barrels ($P < 0.01$ between all clusters, Table 2). However, dendrites of MC1 interneurons rarely showed projections to the supra- or infra-granular layers. The dendritic arbor was typically multipolar, with 4–7 primary dendrites. In most cases (7 out of 8), the soma was positioned in the lower third of the barrel (data not shown).

Morphological Cluster 2: Local Projection Neurons

The second cluster, MC2, comprised 28 interneurons and constituted 58% of our L4 nFS interneuron population. A large fraction of the axon collaterals was confined to the home barrel (58.2 ± 14.6%) and rarely projected outside the home barrel column (93.2 ± 7.3%; see Fig. 2*D*,*E*, Supplementary Video 2). MC2 could be subdivided into 2 sub-categories (MC2a and MC2b) that exhibited differences in the axonal projection patterns in the home barrel column.

The first subgroup, MC2a, comprised 20 nFS interneurons. The average total axonal length of these interneurons was 35 ± 10 mm, and the average total dendritic length was 4.2 ±

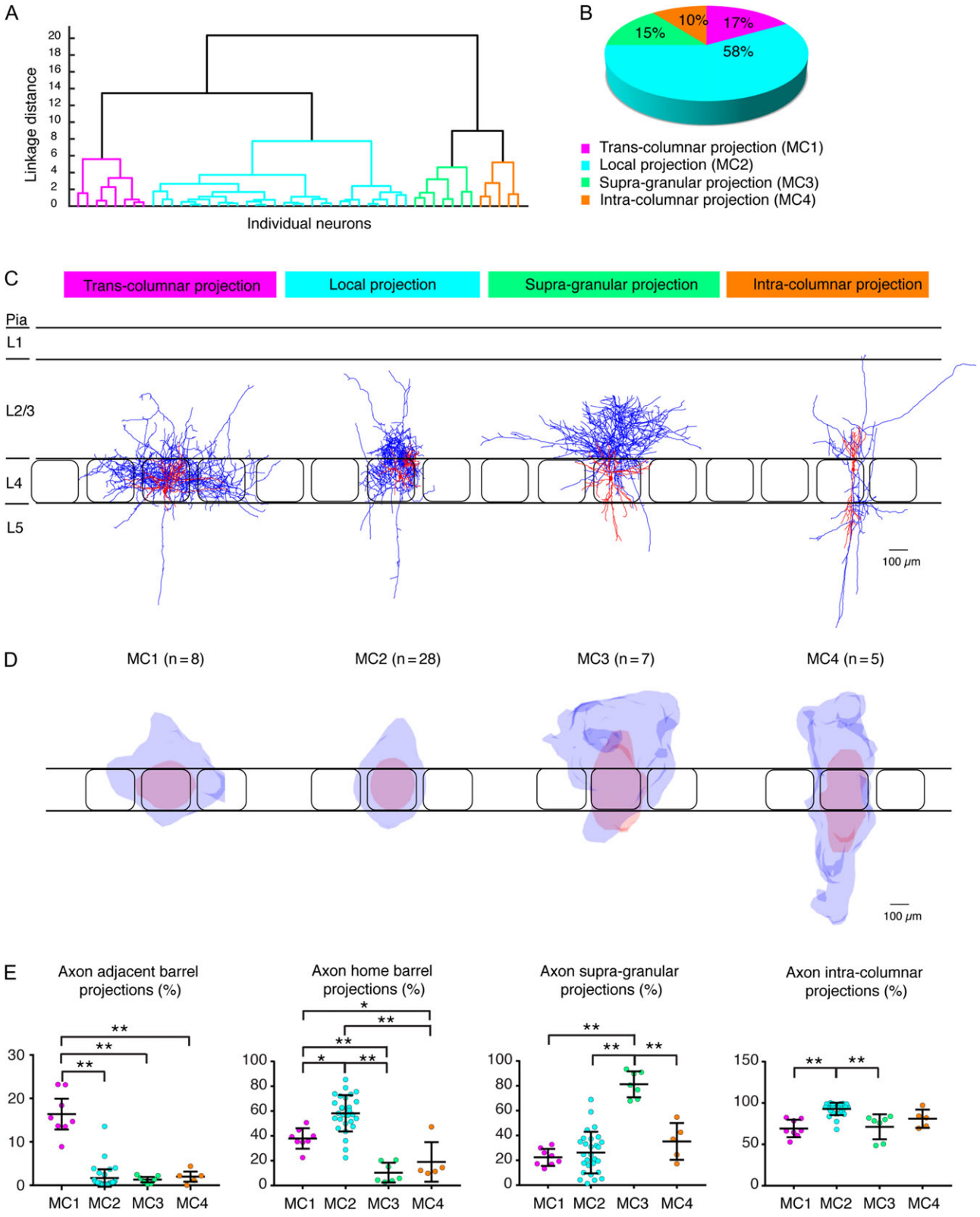

Figure 2. Quantitative morphological classification of L4 nFS interneurons in rat barrel cortex. (*A*) Ward's method of unsupervised hierarchical cluster analysis was used to identify different clusters from 48 nFS interneurons based on morphological parameters listed in Table 1. The x-axis of dendrogram shows individual neurons, and the y-axis corresponds to the linkage distance measured by Euclidean distance. Cluster 1 (MC1) is shown in magenta, cluster 2 (MC2) in light blue, cluster 3 (MC3) in green, and cluster 4 (MC4) in orange. All the figures here follow the same color code. (*B*) The pie chart shows the percentage contribution of each cluster. (*C*) Representative examples for the 4 morphological clusters revealed by unsupervised cluster analysis. Axons are labeled in blue, and the somatodendritic domain in red. (*D*) The 80-percentile of integrated axonal (blue) and dendritic (red) length density. The axons and dendrites were aligned with respect to the soma position, (*E*) Scatter box plot describing significant differences between 3 clusters. Significance is represented as $^{*}P < 0.05$, $^{**}P < 0.01$.

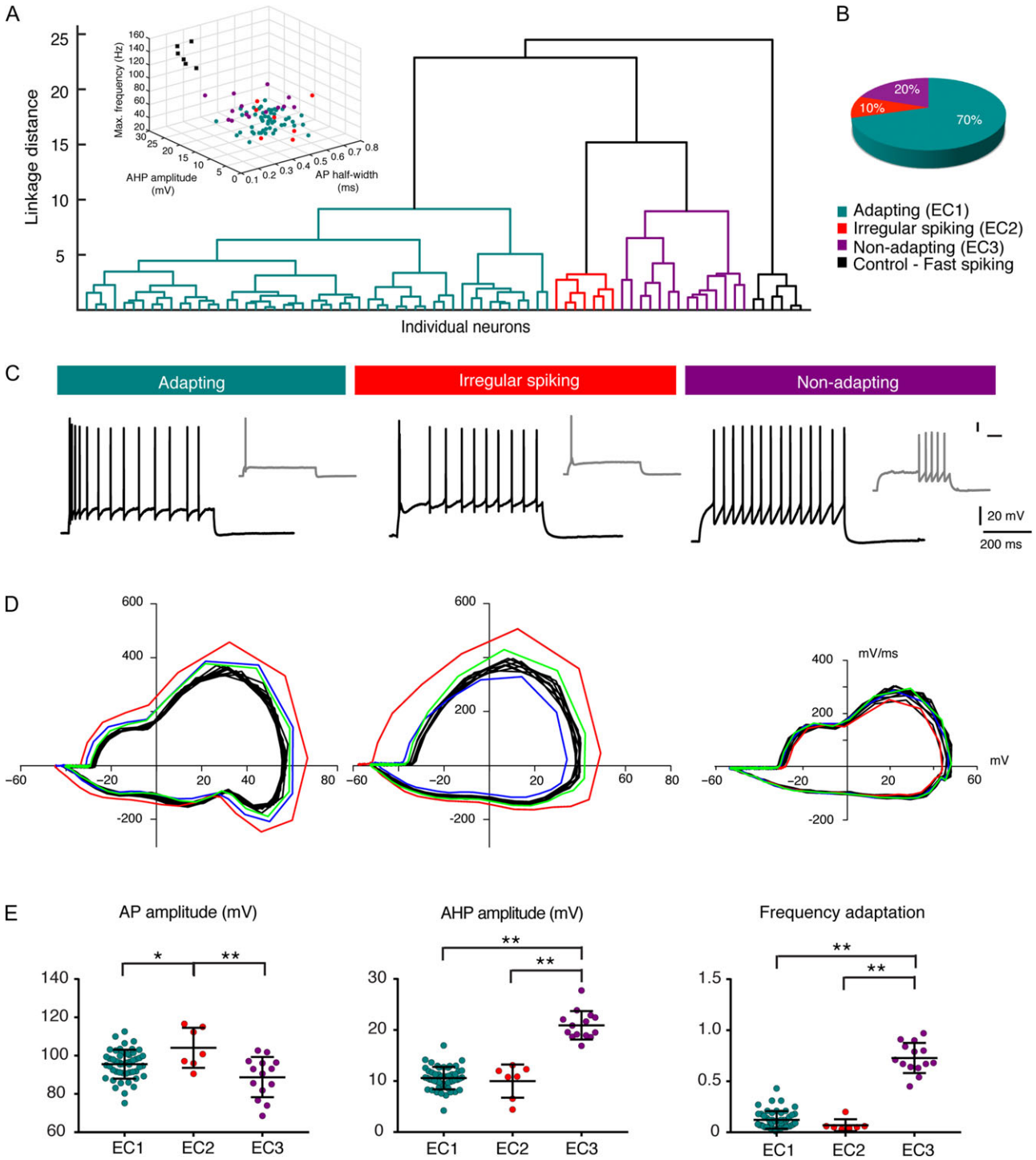

Figure 3. Quantitative electrophysiological classification of L4 nFS interneurons in rat barrel cortex. (*A*) Ward's method of hierarchical cluster analysis was used to identify different clusters from 71 nFS interneurons based on passive membrane properties, AP and firing properties. The x-axis of dendrogram shows individual neurons, and the y-axis corresponds to the linkage distance measured by Euclidean distance. FS interneurons were used as controls and were clearly separated as 1 cluster (black). Cluster 1 (EC1) is shown in teal, Cluster 2 (EC2) in red, and Cluster 3 (EC3) in purple. (inset) 3D scatter plot showing the clear separation of FS and nFS interneurons. (*B*) The pie chart shows the percentage contribution of each cluster. (*C*) Representative firing patterns for each cluster, showing 10-spike trains. The first AP(s) at rheobase current injection is shown in gray. (*D*) Phase plots of representative EC1, EC2, and EC3 interneuron firing patterns. The first, second, and third spikes are labeled in red, blue and green, respectively. (*E*) Scatter box plot describing various passive membrane properties, AP, and firing properties of 71 nFS interneurons in Layer 4 of rat barrel cortex that shows significant difference between 3 clusters. Significance is represented as $^{*}P < 0.05$, $^{**}P < 0.01$.

1.0 mm. The characteristic feature of this cluster was their dense local axonal plexus that was largely confined to the home barrel (64.2 ± 11.1%), with some projections to supra-, and only a few to infra-granular layers (19.2 ± 11.9% and 6.9 ± 5.8%, respectively). Dendrites displayed a multipolar projection pattern; extensive branching within the home barrel (93.2 ± 5.6%), and little to no collaterals in supra- and infra-granular layers (Fig. 2*D*, Supplementary Fig. 3*B*).

Table 2 Statistical analysis for the morphological parameters of L4 nFS interneurons

Parameters (%)	MC1	MC2	MC3	MC4	MC1 vs. MC2	MC1 vs. MC3	MC1 vs. MC4	MC2 vs. MC3	MC2 vs. MC4	MC3 vs. MC4
Axon supra-granular	22.37 ± 6.87	26.21 ± 16.76	81.27 ± 10.47	35.20 ± 14.83	ns	<0.1	ns	<0.1	ns	<0.1
Axon Layer 4	69.07 ± 7.42	67.03 ± 15.36	14.62 ± 10.79	27.49 ± 22.74	ns	<0.1	<0.1	<0.1	<0.1	ns
Axon infra-granular	8.73 ± 5.00	6.44 ± 5.16	4.09 ± 4.28	34.49 ± 13.25	ns	ns	<0.1	ns	<0.1	<0.1
Axon home barrel	37.96 ± 8.21	58.20 ± 14.66	10.40 ± 7.97	19.04 ± 15.89	<0.5	<0.1	<0.5	<0.1	<0.1	ns
Axon adjacent barrel	16.38 ± 4.96	1.67 ± 2.83	1.30 ± 0.85	1.98 ± 1.62	<0.1	<0.1	<0.1	ns	ns	ns
Axon intra-columnar	69.11 ± 10.61	92.81 ± 7.49	71.22 ± 15.07	80.91 ± 11.01	<0.1	ns	ns	<0.1	ns	ns
Dendrites supra-granular	1.49 ± 1.99	7.32 ± 10.28	33.10 ± 13.42	22.80 ± 15.91	ns	<0.1	<0.1	<0.1	<0.5	ns
Dendrites Layer 4	88.32 ± 15.09	92.64 ± 10.98	50.96 ± 15.23	41.74 ± 24.05	ns	<0.1	<0.1	<0.1	<0.1	ns
Dendrites infra-granular	5.08 ± 6.00	0.71 ± 1.47	24.77 ± 19.16	35.36 ± 25.07	ns	<0.1	<0.1	<0.1	<0.1	ns
Dendrites home barrel	70.62 ± 12.21	87.48 ± 11.26	41.71 ± 15.46	32.87 ± 17.31	ns	<0.1	<0.1	<0.1	<0.1	ns
Dendrites adjacent barrel	6.00 ± 8.14	0.11 ± 0.31	1.43 ± 2.30	1.40 ± 1.67	<0.1	<0.5	<0.5	ns	ns	ns
Dendrites intra-columnar	85.38 ± 15.00	99.21 ± 1.60	93.43 ± 7.07	97.00 ± 3.08	<0.1	ns	<0.1	ns	ns	ns

All data are represented as mean ± standard deviation. Statistical significance between all the clusters were performed using one-way ANOVA test, and Tukey test was performed for the significant difference between individual clusters.

The second subgroup, MC2b, consisted of 8 nFS interneurons with an average axonal length of 37.3 ± 6.0 mm and an average dendritic length of 4.3 ± 0.6 mm. Although the axons of MC2b interneurons were largely confined to the home column, only 49.9 ± 12.3% of the axonal branches were located in Layer 4. A significant fraction of axonal collaterals (43.6 ± 14.5%) ascended to Layers 2/3 and 1, and few descended to Layer 5 (5.1 ± 2.8%). Unlike MC2a, a significant percentage (21.1 ± 9.0%) of MC2b interneuron dendrites projected to supra-granular layers. The cell bodies of all MC2b interneurons were mainly found in the upper half of the barrel (Fig. 2*D*, Supplementary Fig. 3*C*).

Morphological Cluster 3: Supra-granular Projection Neurons

Cluster 3 (MC3) comprised 7 interneurons and constituted 15% of the total nFS interneurons analyzed in our study. A characteristic feature of this cluster was that axons projected mainly outside the home barrel and innervated Layer 2/3 extensively (Fig. 2*D*–*F*, Supplementary Video 3). MC3 interneurons had a high average total axonal length of about 40 ± 12 mm, most of which was confined to the supra-granular layers (81.2 ± 10.5%). Only 10.4 ± 8% of the total axon branches were found in the home barrel, which was markedly different from interneurons of the other 3 clusters. MC3 axons projected horizontally in Layer 2/3, with ~30% outside the home column (Fig. 2*D*,*E*). MC3 interneuron dendrites showed a bipolar or multipolar appearance.

Morphological Cluster 4: Intra-columnar Projection Neurons

The last cluster, MC4, comprised 5 interneurons and constituted 10% of the total nFS interneurons analyzed. They showed morphological features similar to those of classical VIP+ interneurons (Fig. 2*D*,*E*, Supplementary Video 4) (Porter et al. 1998; Pronneke et al. 2015). MC4 interneurons had a low number of axonal collaterals, with an average total axonal length of only 25.4 ± 15 mm, the lowest in our L4 nFS interneuron population. A roughly equal fraction of axonal collaterals of the MC4 interneurons was found in supra- and infra-granular layers (35.2 ± 14.8% and 34.5 ± 13.2%, respectively); ~20% of the axons were located in the home barrel. Dendrites of MC4 interneurons were bipolar, and showed an extra-granular projection pattern similar to that of their axons.

Electrophysiological Classification of nFS Interneurons

For the electrophysiological analysis, 71 L4 nFS interneurons were examined. The electrophysiological classification of nFS interneurons was based on their passive electrophysiological properties, single AP features, and repetitive firing characteristics. As a control group, 6 FS interneurons were also included in the classification. Overall, L4 nFS interneurons showed very heterogeneous firing patterns (Supplementary Fig. 4).

Based on the parameters listed in Table 1, we performed a CA on the dataset of 77 (71 nFS and 6 FS interneurons) single-cell recordings in the PC space to classify L4 nFS interneurons. The first 4 PCs with eigenvalues greater than 1 were retained for cluster analysis. The percentage of variance explained by 4 PCs was about 74%. The relative contribution of the parameters is listed in Supplementary Table 4. Unsupervised hierarchical CA revealed 3 distinct electrophysiological clusters of nFS interneurons, with FS interneurons as a clear fourth cluster (Fig. 3A, Supplementary Fig. 4). Using 3 electrophysiological parameters, i.e., the AP half-width, the maximum firing frequency and the AHP amplitude, FS interneurons were reliably distinguished from nFS interneurons without any overlap between the 2 interneuron classes (Fig. 3A, inset). Cluster 1 (EC1) comprised 50 nFS interneurons, was highly heterogenous, and included many distinct subgroups. EC1

interneurons constituted 70% of the total population and showed strong adaptation; Cluster 2 (EC2) comprised 10% of the total population and displayed a characteristic initial burst followed by a irregular spiking behavior; Cluster 3 (EC3) amounted to 20% of the total population and showed regular spiking non-adapting firing pattern (Fig. 3B,D). The validation of hierarchical clustering was made using K-means clustering with K equal to the number of clusters obtained from the average silhouette width showing the largest value. The clusters obtained by hierarchical clustering and K-means were almost identical with the exception of 1 misalignment (Supplementary Table 1).

Electrophysiological Cluster 1: Adapting Neurons

EC1 constituted the largest group of nFS interneurons, comprising of 50 interneurons, i.e., 70% of the total nFS interneurons. A characteristic feature of this cluster was their high-frequency adaptation (Fig. 3C; Table 3). The frequency adaptation of 0.12 ± 0.09 (calculated as the ratio of the first ISI and the last ISI in a 10-spike train) reflected extremely strong adaptation (Fig. 3C,E).

Although EC1 interneurons were characterized by a more depolarized V_{rest} (–61.7 ± 4.2 mV) and AP threshold (–39.0 ± 3.5 mV), they displayed a significantly lower R_{in} (70.5 ± 19.7 MΩ) suggesting the existence of a large number of open leak channels which in turn would reduce neuronal excitability (rheobase current: 226.9 ± 92.4 pA) and resulted in a fast membrane time constant (τ_m: 8.1 ± 2.2 ms). The large sag index of 12.3 ± 5.9 suggests a high density of hyperolarization-activated cyclic nucleotide-gated (HCN) channels, which may also contribute to the depolarized V_{rest}.

The half-width of APs was much longer compared to the FS interneurons (0.44 ± 0.08 vs. 0.20 ± 0.03 ms). To better examine the AP properties, we used phase plots in which the rate of change of the membrane potential with respect to time (dV/dt) was plotted as a function of the membrane potential (V_{rest}) (Fig. 3D). For EC1 interneurons, the phase plot revealed a rapid spike onset and exhibited a biphasic component during the rising phase of the AP. The first AP displayed the largest amplitude, while the subsequent ones showed gradual amplitude accommodation. EC1 interneurons exhibited the strongest amplitude accommodation (6.9 ± 3 mV), which was calculated as the difference between the average of the first and last 3 AP peak amplitudes. The average AHP amplitude of EC1 interneurons was 10.6 ± 2.2 mV.

Electrophysiological Cluster 2: Irregular Spiking Neurons

EC2 was the smallest cluster, consisting of only 7 interneurons. One of the characteristic features of EC2 interneurons was an initial burst of 2 or 3 APs followed by a relatively long ISI (Fig. 3C).

EC2 neurons displayed extremely high R_{in} (226.1 ± 36.3 MΩ), with a V_{rest} of –71.4 ± 3.1 mV and an AP threshold of –43.6 ± 2.9 mV. Therefore, the rheobase current was small (77.1 ± 23.6 pA) and τ_m relatively slow (13.5 ± 2.2 ms). The small sag index was indicative of a low HCN channel expression in EC2 interneurons (sag index: 3.0 ± 1.8).

EC2 interneurons displayed the highest AP amplitude (104.1 ± 10.4 mV) probably because of their negative V_{rest}, which facilitates the recovery of Na^+ channels from inactivation, compared to the other clusters, whereas their AHP amplitude was relatively small (10 ± 3.2 mV) (Table. 3). For every current injection, the initial spike in an AP train always had the fastest rate of rise while the second spike displayed without exception the smallest AP amplitude and slowest rate of rise, as can be seen in the phase plot displaying the 10-spike train (first and second traces in red and blue colors, respectively) (Fig. 3D). The phase plot revealed a monophasic component during the rising phase of the AP.

Electrophysiological Cluster 3: Non-adapting Neurons

EC3 represented a regular spiking, non-adapting group of nFS interneurons, which constituted around 20% of the total population. Some interneurons of this cluster displayed late-spiking behavior, which has been described to be characteristic for NGFCs (Chittajallu et al. 2013). An adaptation ratio of 0.7 ± 0.1 indicates a weak adapting firing pattern of the EC3 interneurons (Fig. 3E; Table 3).

The V_{rest} of EC3 interneurons was –67.6 ± 4.5 mV, and the AP threshold was –33.9 ± 5.4 mV. EC3 interneurons had a high R_{in} (151.3 ± 49.3 MΩ), a slow membrane time constant (τ_m: 12.5 ±

Table 3 Statistical analysis for the electrophysiological parameters of L4 nFS interneurons

Parameters	EC1	EC2	EC3	EC1 vs. EC2	EC1 vs. EC3	EC2 vs. EC3
Resting membrane potential, V_{rest} (mV)	–61.76 ± 4.18	–71.43 ± 3.15	–67.64 ± 4.53	<0.01	<0.01	ns
Input resistance, R_{in} (MΩ)	70.48 ± 19.75	226.15 ± 36.31	151.28 ± 49.26	<0.01	<0.01	ns
Voltage sag (%)	12.31 ± 5.91	3.03 ± 1.76	6.26 ± 5.66	<0.01	<0.05	ns
Membrane time constant, τ_m (ms)	8.10 ± 2.25	13.51 ± 2.22	12.55 ± 6.11	<0.01	<0.01	ns
Rheobase (pA)	226.90 ± 92.35	77.14 ± 23.60	166.43 ± 65.00	<0.01	ns	<0.05
AP threshold (mV)	–39.00 ± 3.50	–43.65 ± 2.90	–33.93 ± 5.37	<0.01	<0.01	<0.01
AP amplitude (mV)	95.56 ± 7.51	104.10 ± 10.44	88.78 ± 10.50	<0.05	ns	<0.01
AP half-width (ms)	0.44 ± 0.08	0.50 ± 0.12	0.55 ± 0.15	ns	<0.05	ns
AP latency (ms)	102.40 ± 26.34	119.92 ± 45.47	319.24 ± 245.17	ns	<0.01	<0.01
AHP amplitude (mV)	10.58 ± 2.19	10.00 ± 3.25	20.92 ± 2.79	ns	<0.01	<0.01
AP amplitude accommodation (mV)	6.86 ± 3.01	0.52 ± 3.04	2.74 ± 2.16	<0.01	<0.01	ns
Average of inter-spike interval, ISI (ms)	80.94 ± 12.42	76.64 ± 17.29	77.95 ± 14.66	ns	ns	ns
CV of ISI (ms)	0.78 ± 0.34	0.45 ± 0.14	0.12 ± 0.07	<0.05	<0.01	<0.05
Frequency adaptation ISI_1/ISI_9	0.12 ± 0.09	0.07 ± 0.06	0.73 ± 0.15	ns	<0.01	<0.01
Frequency adaptation ISI_{min}/ISI_{max}	0.09 ± 0.06	0.05 ± 0.05	0.65 ± 0.14	ns	<0.01	<0.01
Frequency-current slope (Hz/pA)	16.32 ± 5.37	18.02 ± 6.64	11.74 ± 4.81	ns	ns	<0.05
Maximum firing frequency (Hz)	52.66 ± 14.78	52.86 ± 20.51	44.86 ± 15.73	ns	ns	ns

All data are represented as mean ± standard deviation. Statistical significance between all the clusters were performed using one-way ANOVA test, and Tukey test was performed for the significant difference between individual clusters.

6.1 ms), and a small sag index value (6.3 ± 5.7). The rheobase current was 166.4 ± 65 pA.

The phase plot of EC3 interneurons revealed a delayed onset of the AP and a biphasic component at the rising phase of the AP (Fig. 5D). EC3 interneurons displayed a low firing frequency per 100 pA current injection (11.7 ± 4.8 Hz). Characteristic features of EC3 interneurons were a broad AP width (0.55 ± 0.1 ms) and a large AHP amplitude (20.9 ± 2.8 mV). While the AHP amplitude in EC3 interneurons was very similar to that of FS interneurons (24.0 ± 3.1 mV) and differed significantly from that of EC1 and EC2, the AP half-width was much longer compared to FS interneurons. EC3 interneurons exhibited APs with a small amplitude of 88.8 ± 10.5 mV.

Correlation Between Morphological and Electrophysiological Clusters

About 4 morphological and 3 electrophysiological clusters of nFS interneurons in Layer 4 of rat barrel cortex were identified quantitatively using unsupervised hierarchical CA. We tried to determine if the morphological and electrophysiological properties were correlated.

To this end, we used those cells for which we had obtained both high-quality electrophysiological recording and 3D reconstructions. However, the number of nFS interneurons in this dataset was only 28 because a dataset with a high-quality electrophysiological recording may not have a complete biocytin-filling resulting in a poor or no morphological reconstruction. Similarly, a recording may not be included in the dataset because of poor access or instability despite showing an excellent biocytin staining. Therefore, not all the morphological reconstructions had their corresponding electrophysiological data, and vice versa.

We performed an unsupervised hierarchical CA on these 28 nFS interneurons including both morphological and electrophysiological parameters. The combined morphological-electrophysiological clusters (MECs) revealed 5 different L4 nFS interneuron types (Fig. 4A,B, Supplementary Fig. 5).

MEC1 interneurons are morphologically identical to MC1 interneurons that show a trans-columnar axonal projection; their electrophysiological properties are similar to those of EC1 interneurons with an adapting firing behavior (Fig. 4C). MEC2 was the largest group, corresponding to the MC2 interneurons showing local projection and EC1 interneurons with adapting firing behavior. MEC3 was one of the smallest clusters with only 2 neurons,

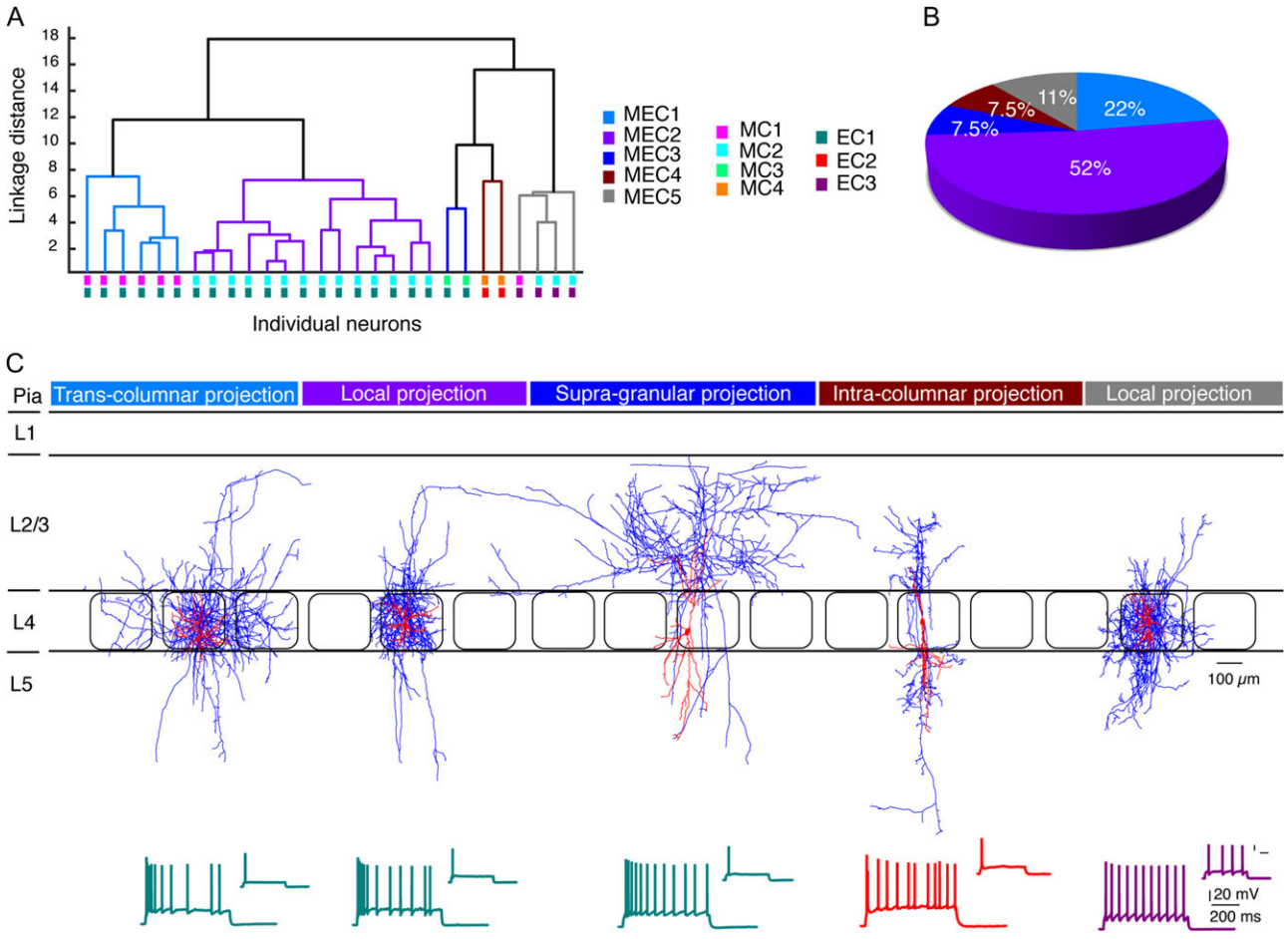

Figure 4. Comparison of morphological and electrophysiological clusters. Combined unsupervised hierarchical clustering based on both morphological and electrophysiological parameters revealed 5 distinct clusters. The colored bars beneath each dendrogram represent the color code from the morphological and electrophysiological dendrograms (see Figs 2 and 3). (*B*) The pie chart shows percentage contribution of each cluster. (C) Representative examples of L4 nFS interneurons of the 5 clusters revealed by unsupervised cluster analysis based on morphological/electrophysiological parameters. Axons are labeled in blue, and the somatodendritic domain in red. The firing pattern corresponding to the example morphologies have the same color code as in Fig. 3.

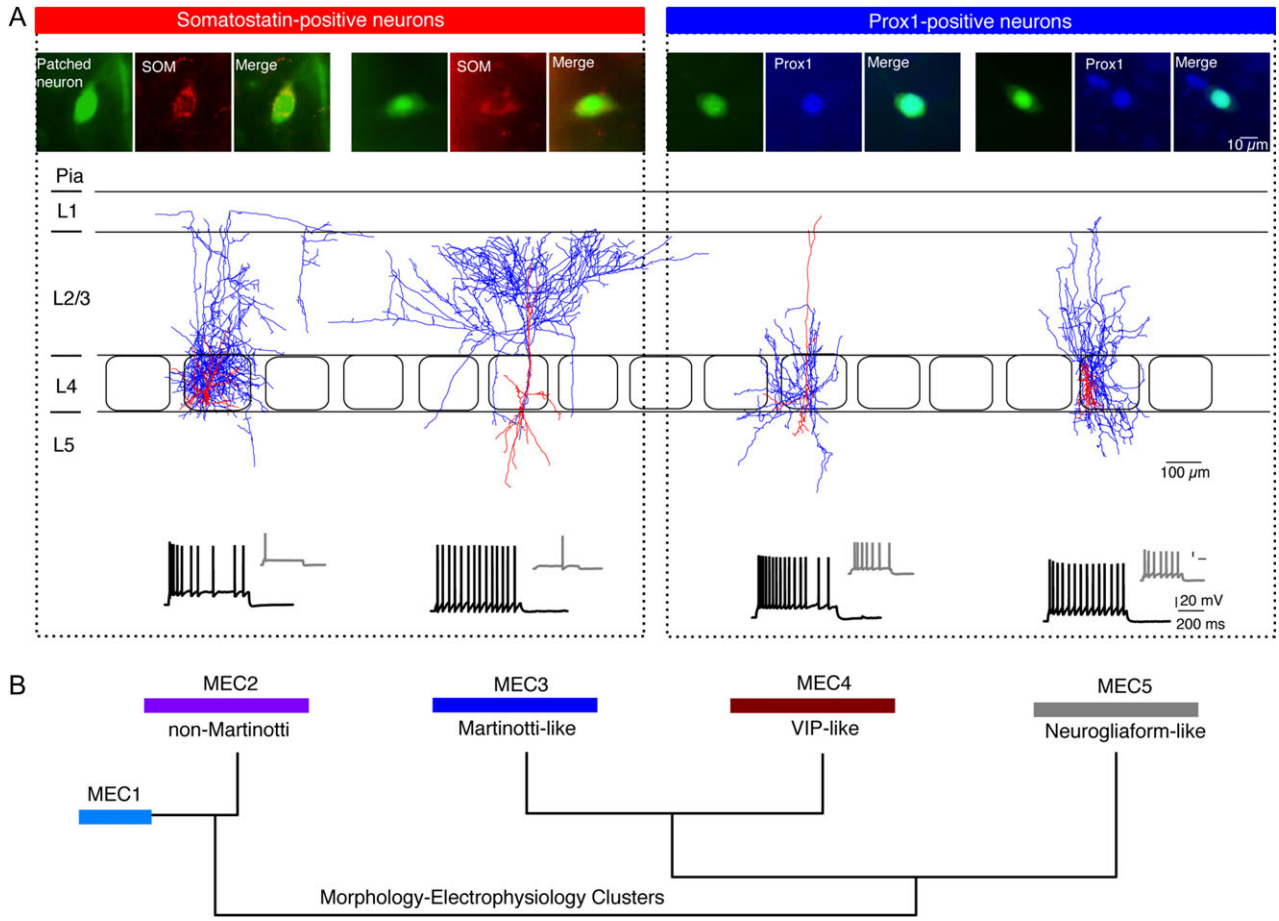

Figure 5. Neurochemical marker identification of L4 nFS interneurons in rat barrel cortex. (*A*) L4 nFS interneurons recorded using whole-cell patch-clamp technique were filled with biocytin coupled to Alexa 488 (green) to identify the location and morphology of patched neurons and tested for the co-localization of somatostatin (red) or Prox1 (blue) expression. Representative examples of nFS interneurons expressing somatostatin (left) and Prox1 (right) with their morphological identities and firing pattern are shown. Axon is labeled in blue, soma and dendrites in red. (*B*) All 4 neurons belonged to 1 of the 5 clusters revealed by combined morphological-electrophysiological classification.

displaying supra-granular projection (MC3) and adapting firing pattern (EC1). The fourth cluster, MEC4, corresponded to the intra-columnar projection interneurons showing VIP-like morphologies (MC4). Electrophysiologically, they were correlated with EC2 interneurons displaying irregular spiking behavior. The last cluster, MEC5, corresponded to the subgroup of MC2 interneurons with a morphology similar to that of NGFCs (Chittajallu et al. 2013) and displayed regular spiking non-adapting firing behavior (EC3). Most of the neurons in MECs were assigned similarly to the MCs, with an addition of 1 new cluster.

Neurochemical Expression of nFS Interneurons in Layer 4

To identify the expression of molecular markers of single L4 nFS interneurons in brain slices and to correlate them with the electrophysiological and morphological properties, we combined patch-clamp recording with simultaneous filling of biocytin and the fluorescent Alexa dye (n = 20). After successful recording and PFA fixation, brain slices were processed for PV, SOM, Prox1 (a surrogate marker that labels caudal ganglionic eminence (CGE)-derived 5-HT_{3a}R expressing interneurons, see Miyoshi et al., 2010 for details) and VIP (Supplementary Fig. 6). Finally, the morphology of the labeled neurons was revealed using the biocytin-DAB histochemistry.

Out of the 20 L4 nFS interneurons, 14 nFS interneurons were SOM-positive but Prox1-negative, and 3 nFS interneurons were Prox1-positive and SOM-negative (Fig. 5A). Three nFS interneurons showed no immunoreactivity for either SOM or Prox1. Some control experiments were performed on FS interneurons, all of which were PV-positive (data not shown). Neurons with clear background labeling and only few truncations were reconstructed to identify their morphology. Eight SOM-positive interneurons were morphologically reconstructed; they belonged to either MEC2 or MEC3 and displayed either a mainly local projection pattern (non-Martinotti cells) or a largely supra-granular projection (Martinotti-like interneurons) with adaptive firing behavior (Fig. 5A,B, Supplementary Fig. 7). One Prox1-positive neuron belonged to MEC4 displaying VIP-like morphology with irregular firing behavior. Two of the three Prox1-positive neurons belonged to MEC5 (NGFCs showing regular spiking non-adapting firing behavior). Except MEC1, all the clusters were identified with a molecular marker expression.

Discussion

In this study, we have investigated the different nFS interneuron types and their electrophysiological properties in the L4 neuronal microcircuitry of rat barrel cortex. We found that L4 nFS interneuron types show a large degree of morphological

and electrophysiological diversity. Using unsupervised hierarchical CA on a combination of morphological and electrophysiological parameters, we identified 5 distinct types of nFS interneurons in Layer 4: 1) *trans-columnar projecting interneurons*, 2) *locally projecting non-Martinotti-like interneurons*, 3) *supragranular projecting Martinotti-like interneurons*, 4) *intra-columnar projecting VIP-like interneurons, and* 5) *locally projecting NGFC-like interneurons*.

We identified a novel type of interneuron that has not been described previously, which showed extensive axonal arborizations not only in their home barrel but also in the adjacent barrels. Furthermore, an analysis of the molecular marker expression indicated that most of the L4 nFS interneurons (70%) were SOM-positive and few (15%) were positive for Prox1, a surrogate marker for 5-HT_{3a}R expressing interneuron group.

Classification of Interneurons Based on Quantifiable Morphological and Electrophysiological Parameters

Given the diversity of interneuron types, it is important to translate the diversity into functional specificity (Gupta et al. 2000; Ascoli et al. 2008; DeFelipe et al. 2013; Kepecs and Fishell 2014; Zeng and Sanes 2017). In order to better characterize the heterogenous population of neocortical interneurons, several parameters describing axonal and dendritic geometry, intrinsic properties, and protein expression have been used in interneuron classification studies. Given the ample number of possible parameters for a classification of interneurons, it is important to consider those that are functionally relevant and sufficiently stable over time.

Recent studies on neuronal classification were performed using morphological parameters such as fractal analysis, Sholl analysis, fan-in analysis and so on (McGarry et al. 2010; Muralidhar et al. 2013; Santana et al. 2013). To investigate how these analysis methods can help to identify interneuron subtypes, we performed an unsupervised hierarchical CA on the 48 nFS interneurons used in this study. This CA was based on 64 morphological parameters extracted from the Neuroexplorer, including features of the soma, dendrites, and axon (for a full list, see Supplementary Table 5). It resulted in a scrambled distribution of interneuron morphologies, i.e., interneurons with widely different axonal projection patterns were grouped into a single cluster so that no meaningful information with respect to their morphological properties and potential synaptic connectivity could be extracted (Supplementary Fig. 8). Therefore, it is important to consider those parameters that allow a prediction of the potential synaptic connectivity, i.e., those that define innervation domains. Innervation domains are defined by the axo-dendritic overlap extracted from the 3D neurite path length density maps. They provide information about the innervation density (Lubke et al. 2003; Helmstaedter and Feldmeyer 2010) and hence the potential of synapse formation with surrounding excitatory and inhibitory neurons (but see Rees et al., 2017 for a discussion of innervation and axo-dendritic overlap). Because neuronal cell types can generally not be identified by single features, ideally electrophysiological parameters and molecular marker expression should also be used as criteria for the classification of different interneuron types.

The basic question of how distinct interneuron classes are (Parra et al. 1998), or how to approach the continuum of phenotypes (Battaglia et al. 2013) remains open. One of the most commonly used unsupervised CA methods in interneuron classification is Ward's hierarchical CA. This method uses an approach, which merges nearest clusters at each step. We validated the quality of this clustering using the silhouette method. To test the robustness of the classification, we also compared the results of unsupervised clustering algorithm with an alternate supervised clustering method such as K-means clustering which is a top-down cluster analysis method. Using these different methods, we were able to ascertain the reliability of our cluster assignments.

Different Types of L4 nFS Interneurons and their Possible Functional Roles

Unsupervised hierarchical CA of L4 nFS interneurons based on the morphological parameters alone yielded 4 independent clusters (MC1–MC4), whereas the electrophysiological parameters generated 3 independent clusters (EC1–EC3). Combining morphological and electrophysiological parameters produced clusters similar to the morphological clusters, except for a MC sub-cluster that separated out as an individual cluster, thus altogether resulting in 5 independent clusters (MEC1–MEC5). The morphological parameters gave a meaningful description of the L4 nFS interneuron types but the electrophysiological properties helped to identify subgroups when combined with the morphological parameters. CA based on electrophysiological properties and AP firing patterns alone did not yield a useful classification, because 3 morphologically distinct nFS interneuron types showed similar firing patterns (Fig. 4*C*). However, partial correlation between the morphological and electrophysiological clusters appeared to exist.

Such a partial correlation between morphology and electrophysiological subtypes was found for MEC5 NGFC-like interneurons, which are a sub-cluster of MC2 local projecting interneurons with a EC3 regular spiking non-adapting firing pattern (Fig. 4*A*,*C*). In addition, MC4 interneurons with VIP-like morphology were correlated with EC2 interneurons with initial bursting followed by irregular spiking. This AP firing behavior has been associated with a bipolar somatodendritic geometry (Helmstaedter et al. 2009a,c) and has been described for a bipolar L2/3 trans-laminar interneuron type resembling a VIP-expressing interneuron.

The problem of finding a well-defined correlation between morphology and AP firing pattern has been noted previously (Markram et al. 2004) and may be due to several reasons. It is conceivable that subtle differences in the ion channel complement of neurons within defined clusters exist which cannot be resolved here. Furthermore, the firing pattern is highly dynamic. It depends to a certain degree on external conditions such as preceding or on-going neuronal activity and/or the activity of neuromodulators which are often present at low background concentrations even in brain slice preparations thereby exerting a tonic influence, see e.g., (Kolomiets et al. 2009; Bartlett et al. 2011; Qi et al. 2017) and may alter single APs and AP firing patterns by affecting e.g., K^+ and Ca^{2+} channels. This may result in recording variable firing patterns in the same neuron type.

L4 MEC1 Trans-columnar Projecting Interneurons

Trans-columnar projecting MEC1 interneurons are a novel interneuron type and have not been described in previous studies. Their most characteristic feature is their extensive axonal collateralization in directly adjacent, primary surround barrels and to some extent even in secondary surround barrels. The functional role of this interneuron type is likely to be the inhibition of excitatory neurons in the neighboring barrels. In several publications, barrels in Layer 4 have been described as functionally independent structures that receive little or no direct excitatory nor inhibitory synaptic inputs from adjacent barrels (Petersen and Sakmann 2001; Laaris and Keller 2002). In

contrast, our findings indicate that the lateral axonal collaterals of L4 MEC1 interneurons may serve to directly inhibit neurons in neighboring barrels in a feed-forward fashion. Thus, these interneurons may be an anatomical correlate for lateral or "surround" inhibition in Layer 4 of the somatosensory barrel cortex (Sachdev et al. 2012).

In the visual cortex, lateral inhibition is known to provide surround suppression of neuronal activity, thereby enhancing sensitivity to contrast edges and eliminating redundant information in the visual environment (Jones et al. 2001; Smith 2006). It has been proposed that SOM-positive interneurons in Layer 2/3 mediate surround inhibition in this sensory area (Adesnik et al. 2012). Recently, lateral inhibition mediated by Layer 2/3 SOM-positive interneurons was also demonstrated in the auditory cortex (Li et al. 2014; Kato et al. 2017).

In the somatosensory barrel cortex, suppression of the neuronal activity in surround barrels may be involved in contrast enhancement of principal whisker signaling (Brumberg et al. 1996; Derdikman et al. 2003; Sachdev et al. 2012). Several studies show that surround whisker responses are suppressed by the co-stimulation or stimulation of one whisker followed by the other (Garabedian et al. 2003; Drew and Feldman 2007; Boloori et al. 2010). However, the underlying mechanisms of lateral (surround) inhibition and its cellular basis are not well understood. Previous studies have demonstrated the existence of laterally projecting interneurons in Layer 2/3 (Helmstaedter et al. 2009b) but such interneurons have not been found in Layer 4. The data presented here suggest that lateral inhibition in the barrel cortex takes place not only in Layer 2/3 but already at the level of Layer 4, the major thalamorecipient layer. Thus, L4 MEC1 interneurons may act by enhancing the contrast between sensory signals arriving from the principal vs. surround whisker.

A small subset of MEC1 interneurons possesses ascending branches to Layer 2/3 that terminate in Layer 1. Only few MEC1 interneurons have axonal projections to the L5/6 border. This suggests some minor trans-laminar feed-forward signaling of the L4 MEC1 interneurons; however, the low density of these collaterals suggests that this is of low functional relevance. Electrophysiologically, these interneurons were characterized by a high-frequency adaptation, similar to the firing pattern shown for non-Martinotti SOM interneurons in Layer 4 (Ma et al. 2006a; Xu et al. 2013).

L4 MEC2 Locally Projecting Non-Martinotti-like Interneurons

L4 MEC2 interneurons with local axonal projections are the most common type of L4 nFS interneurons. Although MEC2 interneurons show some degree of heterogeneity in their axonal projection pattern, more than 90% of the axonal arbor is confined within the home column, with sparse ascending and descending branches to the superficial and infra-granular layers, respectively. The main feature of MEC2 interneurons is an extremely dense local axon plexus with an average total length of more than 35 ± 10 mm. Such a dense plexus suggests a high connectivity rate to other neurons within the home barrel. This group may correspond to SOM-expressing X94 and non-X94 neurons in Layer 4, the axon of which was also confined to the home barrel (Ma et al. 2006b; Xu et al. 2013). MEC2 interneurons may directly inhibit spiny stellate neurons in Layer 4 or provide disinhibition of spiny stellate neurons by targeting L4 FS interneurons, particularly L4 basket cells which show similarly dense axonal projections within the home barrel (Xu et al. 2013; Koelbl et al. 2015). In preliminary experiments, we found that both L4 nFS and FS interneurons displaying a dense axonal plexus within the home barrel were often reciprocally connected (manuscript in preparation). Because L4 FS basket cells also showed a high degree of connectivity with L4 excitatory neurons (~70%), this suggests the existence of a powerful disinhibitory loop in Layer 4 (Koelbl et al. 2015). These locally projecting interneurons were also characterized by a high-frequency adaptation, similar to MEC1 interneurons.

L4 MEC3 Supra-granular Projecting Martinotti-like Interneurons

The axon of MEC3 interneurons resided primarily in Layer 2/3 of the home and surround barrel columns (84% of the total axonal length of 42 ± 3.5 mm). Only few collaterals are present in Layer 4, thus indicating that only little if any inhibitory connections are established within their home barrel. MEC3 interneurons may provide feed-forward inhibition of the distal dendritic tuft, preferentially of L5B pyramidal cells. The initial bifurcation of the dendritic tuft is the so-called Ca^{2+} spike initiation zone. When a distal, sub-threshold synaptic input occurs coincidentally with Na^{+} AP that back-propagates, this may result in the activation of a Ca^{2+} spike and burst firing of the pyramidal cell. This interaction of the distal Ca^{2+} spike initiation zone with the Na^{+} AP has been proposed to serve as a coincidence detection mechanism that serves to enhance the cortical response to incoming sensory stimuli (Larkum et al. 1999; Larkum and Zhu 2002; Larkum 2013; Major et al. 2013). The axonal projection patterns of MEC3 interneurons are in a suitable position to regulate the association of Na^{+} APs and Ca^{2+} spikes. In addition, MEC3 interneurons may also target the basal dendrites of L2/3 pyramidal neurons. L4 interneurons with a similar axonal projection pattern have been described previously but without specifying whether they were FS or nFS interneurons (Porter et al. 2001). Like MEC1 and MEC2 interneurons, MEC3 interneurons exhibit a strong frequency adaptation.

L4 MEC4 Intra-columnar Projecting VIP-like Interneurons

MEC4 interneurons show morphological features similar to those of VIP-expressing interneurons, with a bitufted dendritic arborization and sparse axonal projections, spanning all layers (Porter et al. 1998; Pronneke et al. 2015; Zhou et al. 2017). Because of their low prevalence, the morphology of VIP interneurons in Layer 4 has not been characterized in detail (but see Pronneke et al., 2015). With an axonal domain that resides mostly outside Layer 4, MEC4 interneurons may inhibit the L2/3 SOM+ interneurons, as reported for L2/3 VIP+ interneurons, thereby disinhibiting the dendritic tufts of L5B pyramidal cells and leading to burst firing of pyramidal cells (Gentet et al. 2012; Karnani et al. 2016; Walker et al. 2016; Muñoz et al. 2017). L4 VIP-like interneurons may also directly inhibit the pyramidal cells arising from supra- and infra-granular layers as suggested by recent findings (Garcia-Junco-Clemente et al. 2017; Zhou et al. 2017). It has been suggested that VIP+ interneurons are also involved in the regulation of cerebral blood flow. Upon stimulation, VIP interneurons together with nitric oxide synthase (NOS)-expressing interneurons release VIP and nitric oxide, which in turn dilates cortical blood vessels, thereby increasing the efficacy of glutamatergic synapses (Pellegri et al. 1998; Cauli et al. 2004).

A subset of MEC4 interneurons displayed an initial burst of APs followed by an accelerated firing upon depolarization. The accelerated firing and decrease in ISI could be due to a slow inactivation of a K^{+} current. It may be involved in the enhancement of synaptic gain and the synchronization of neurons

(Porter et al. 1998; Rozov et al. 2001; Miller et al. 2008; Karagiannis et al. 2009).

L4 MEC5 Locally Projecting Neurogliaform-like Interneurons

MEC5 interneurons show morphological features similar to those of NGFCs that show radially projecting dense axonal plexus and multipolar dendritic arborizations. They display a non-adapting, regular spiking behavior with a broad AP and a large AHP; sometimes they also exhibit a late-spiking behavior (Chu et al. 2003; Oláh et al. 2007; Chittajallu et al. 2013; Jiang et al. 2015). Several studies suggest that a late-spiking firing pattern is indicative of NGFCs (Chu et al. 2003; Zhu and Zhu 2004; Uematsu et al. 2008; Kubota et al. 2011) but we could not confirm this unequivocally. This could be due to the effects of neuromodulation described above.

It has been suggested that NGFCs target excitatory neurons via volume transmission, i.e., not at specialized synaptic contacts (Tamás et al. 2003; Wozny and Williams 2011; Chittajallu et al. 2013). However, they may also elicit slow IPSPs due to their activation of postsynaptic G-protein coupled $GABA_B$ receptors in addition to the $GABA_A$-mediated slow synaptic inhibition (Tamás et al. 2003; Oláh et al. 2007; Capogna and Pearce 2011; Wozny and Williams 2011; Overstreet-Wadiche and McBain 2015).

Relative Percentage of L4 nFS Interneurons and their Molecular Expression

GABAergic interneurons constitute only a small fraction (~12%) of the total number of neocortical neurons. The lowest overall interneuron density (8%) has been reported for Layer 4, which in the rat amounts to 360 interneurons out of a total of approximately 4500 neurons (Meyer et al. 2011). It has been proposed that neocortical interneurons fall into 3 distinct groups, i.e., those expressing PV, SOM, and 5-HT_{3a}R as molecular markers (Rudy et al. 2011). Tremblay and colleagues reported that the majority of L4 interneurons express PV (65%), followed by SOM (16%), and 5-HT_{3a}R (19%) (Tremblay et al. 2016). Since PV is known to be a marker of FS interneurons, the remaining L4 interneurons amount to approximately 3%, or 125 out of a total of 4500 neurons.

In this study, we recorded 105 nFS interneurons, of which a subset of experiments included the identification of molecular markers using immunohistochemistry ($n = 20$). The 5-HT_{3a}R protein, which is selectively expressed in CGE-derived interneurons, shows very low expression levels (Lee et al. 2010; Vucurovic et al. 2010; Zeisel et al. 2015; Tasic et al. 2016) that may not be detected by the antibody labeling used here. Therefore, we used a surrogate marker for 5-HT_{3a}R expressing interneuron group—the transcription factor Prox1, which is expressed in reelin-, VIP-, calretinin-, and neuropeptide Y-positive interneurons (Rubin and Kessaris 2013). Prox1 is specifically required for the maturation and maintenance of CGE-derived interneurons (Miyoshi et al. 2015). In our study, we found that 70% of the L4 nFS interneurons expressed SOM and 15% expressed Prox1. Since Prox1 labels a wide variety of markers, we used a combination of morphological identity and firing pattern to refer to a specific marker. Two of the three Prox1-positive neurons displayed NGFC-like morphology and showed non-adapting firing pattern, which suggests that they express reelin (Miyoshi et al. 2010) (Fig. 5A, Supplementary Fig. 7). One Prox1-positive neuron displayed bipolar dendritic arborization with sparse axon collaterals and irregular firing properties typical for VIP interneurons (Fig. 5A).

The SOM-positive L4 interneurons had a non-Martinotti cell morphology with a local axonal domain (MEC2 interneurons) or were Martinotti-like interneurons with a dominant supragranular projection (MEC3 interneurons; see also Supplementary Fig. 7). In the so-called X94 transgenic mouse line (Ma et al. 2006a; Xu et al. 2013), only SOM-expressing interneurons in Layers 4 and 5B are fluorescence-labeled all of which have been reported to display a non-Martinotti interneuron morphology resembling that of MEC2 interneurons described here. However, in contrast to our findings, no L4 SOM-positive nFS interneurons with a supra-granular axonal projection were found in this transgenic mouse line. This discrepancy could be due to species difference (mouse vs. rat) but is more likely to reflect different SOM expression levels in non-Martinotti and Martinotti L4 nFS interneurons. Thus, in Layer 4 of the barrel cortex, SOM-positive interneurons are more heterogeneous than suggested previously (Xu et al. 2013).

In contrast to interneurons belonging to the MEC2-MEC5 groups, MEC1 interneurons with a largely intra-laminar, transcolumnar axonal projection pattern were not labeled by either Prox1 or SOM antibodies; this may be due to a low expression level of these markers or their complete absence in this particular interneuron type.

It is far from clear how the molecular expression is correlated with the interneuron type. Two large-scale, next-generation RNA-sequencing studies that investigated the expression pattern of multiple molecular markers in neocortical interneurons arrived at conflicting results with respect to the number of identified interneuron types (Zeisel et al. 2015; Tasic et al. 2016). For example, Zeisel and colleagues identified 15 neocortical interneurons of which PV was expressed by only 1, whereas Tasic and colleagues identified 7 PV expressing interneuron types from a total of 23. The most heterogeneous group with respect to marker expression was the 5-HT_{3a}R-positive interneuron group; here, the expression level of the 5-HT_{3a}R differed markedly and was particularly high only in VIP- and reelin-positive interneurons. Thus, it is important to determine to which degree molecular markers can identify functionally distinct interneuron types and how the co-expression of other yet to be determined molecular markers such as transcription factors will contribute to a more specific categorization. A promising approach may be the analysis of gene families that are involved in synapse formation and input-output signaling properties of GABAergic interneurons (such as voltage- and ligand-gated ion-channels, neuromodulator receptors, synapse scaffold proteins, and others). In a recent study (Paul et al. 2017) this has recently been done and led to the identification of different GABergic cell types, however axonal and dendritic properties of interneurons have not been correlated with the "transcriptome" of these neuron types.

Conclusion

Many studies concerning the classification of neocortical GABAergic interneurons have been published in recent years, using several different methodological approaches. As there are several possible analytical methods to classify interneurons, it is important to use functionally relevant parameters as classifiers. In this study, we identified different interneuron motifs based on the axonal projection patterns as the primary classifier, which allowed us to infer their potential synaptic connectivity, thereby providing insights about their possible functional role in intra- and inter-columnar processing of sensory signals. Finally, our methodological approach allowed us to identify a novel interneuron type that has not been described so far and

has not been identified by transgenic approaches. The axonal projection pattern of this neuron type suggest that it is involved in the integration of sensory signals in the barrel cortex. Taken together, our results suggest that even for the small subset of nFS interneurons found in Layer 4 the heterogeneity is remarkably high. To elucidate the functional role of these interneuron types in the neocortex, their actual connectivity profiles and synaptic properties remain to be determined.

Supplementary Material

Supplementary material is available at *Cerebral Cortex* online.

Funding

This work was supported by the Helmholtz Society, the DFG Research Group - BaCoFun (grant no. Fe471/4-2 to D.F.) and the DFG International Research Training Group - 1328 on Schizophrenia and Autism stipend to V.E., the Human Brain Project (to D.F.) and the Natural Science Fund for Colleges and Universities in the Jiangsu Province (grant no. 14KJB140007 to H.W.).

Notes

We thank Werner Hucko for his excellent technical support and Dr. Karlijn van Aerde for custom-written macros in Igor Pro software. We warmly thank Prof. Gord Fishell and Prof. Theofanis Karayannis for their valuable suggestions on immunofluorescence stainings. *Conflict of Interest*: None declared.

References

Adesnik H, Bruns W, Taniguchi H, Huang ZJ, Scanziani M. 2012. A neural circuit for spatial summation in visual cortex. Nature. 490:226–231.

Agmon A, Connors BW. 1991. Thalamocortical responses of mouse somatosensory (barrel) cortex in vitro. Neuroscience. 41:365–379.

Ascoli GA, Alonso-Nanclares L, Anderson SA, Barrionuevo G, Benavides-Piccione R, Burkhalter A, Buzsaki G, Cauli B, Defelipe J, Fairen A, et al. 2008. Petilla terminology: nomenclature of features of GABAergic interneurons of the cerebral cortex. Nat Rev Neurosci. 9:557–568.

Barry PH. 1994. JPCalc, a software package for calculating liquid junction potential corrections in patch-clamp, intracellular, epithelial and bilayer measurements and for correcting junction potential measurements. J Neurosci Methods. 51: 107–116.

Barry PH, Lynch JW. 1991. Liquid junction potentials and small cell effects in patch-clamp analysis. J Membr Biol. 121:101–117.

Bartlett TE, Lu J, Wang YT. 2011. Slice orientation and muscarinic acetylcholine receptor activation determine the involvement of N-methyl D-aspartate receptor subunit GluN2B in hippocampal area CA1 long-term depression. Mol Brain. 4:41.

Battaglia D, Karagiannis A, Gallopin T, Gutch HW, Cauli B. 2013. Beyond the frontiers of neuronal types. Front Neural Circuits. 7:13.

Boloori A-R, Jenks RA, Desbordes G, Stanley GB. 2010. Encoding and decoding cortical representations of tactile features in the vibrissa system. J Neurosci. 30:9990.

Brumberg JC, Pinto DJ, Simons DJ. 1996. Spatial gradients and inhibitory summation in the rat whisker barrel system. J Neurophysiol. 76:130.

Burkhalter A. 2008. Many specialists for suppressing cortical excitation. Front Neurosci. 2:155–167.

Cadwell CR, Palasantza A, Jiang X, Berens P, Deng Q, Yilmaz M, Reimer J, Shen S, Bethge M, Tolias KF. 2016. Electrophysiological, transcriptomic and morphologic profiling of single neurons using Patch-seq. Nat Biotechnol. 34:199–203.

Capogna M, Pearce RA. 2011. GABA A, slow: causes and consequences. Trends Neurosci. 34:101–112.

Cauli B, Tong X-K, Rancillac A, Serluca N, Lambolez B, Rossier J, Hamel E. 2004. Cortical GABA interneurons in neurovascular coupling: relays for subcortical vasoactive pathways. J Neurosci. 24:8940–8949.

Chittajallu R, Pelkey KA, McBain CJ. 2013. Neurogliaform cells dynamically regulate somatosensory integration via synapse-specific modulation. Nat Neurosci. 16:13–15.

Chmielowska J, Carvell GE, Simons DJ. 1989. Spatial organization of thalamocortical and corticothalamic projection systems in the rat SmI barrel cortex. J Comp Neurol. 285: 325–338.

Chu Z, Galarreta M, Hestrin S. 2003. Synaptic interactions of late-spiking neocortical neurons in Layer 1. J Neurosci. 23:96.

Cichon J, Blanck TJJ, Gan W-B, Yang G. 2017. Activation of cortical somatostatin interneurons prevents the development of neuropathic pain. Nat Neurosci. 20(8):1122–1132.

DeFelipe J, Lopez-Cruz PL, Benavides-Piccione R, Bielza C, Larranaga P, Anderson S, Burkhalter A, Cauli B, Fairen A, Feldmeyer D, et al. 2013. New insights into the classification and nomenclature of cortical GABAergic interneurons. Nat Rev Neurosci. 14:202–216.

Derdikman D, Hildesheim R, Ahissar E, Arieli A, Grinvald A. 2003. Imaging spatiotemporal dynamics of surround inhibition in the barrels somatosensory cortex. J Neurosci. 23: 3100–3105.

Dodt H-U, Zieglgänsberger W. 1990. Visualizing unstained neurons in living brain slices by infrared DIC-videomicroscopy. Brain Res. 537:333–336.

Drew PJ, Feldman DE. 2007. Representation of moving wavefronts of whisker deflection in rat somatosensory cortex. J Neurophysiol. 98:1566.

Fabrigar LR, Wegener DT, MacCallum RC, Strahan EJ. 1999. Evaluating the use of exploratory factor analysis in psychological research. Psychol Methods. 4:272.

Feldmeyer D, Egger V, Lubke J, Sakmann B. 1999. Reliable synaptic connections between pairs of excitatory layer 4 neurones within a single 'barrel' of developing rat somatosensory cortex. J Physiol. 521(Pt 1):169–190.

Forgy EW. 1965. Cluster analysis of multivariate data: efficiency vs. interpretability of classifications. Biometrics. 21: 768–769.

Fuzik J, Zeisel A, Mate Z, Calvigioni D, Yanagawa Y, Szabo G, Linnarsson S, Harkany T. 2016. Integration of electrophysiological recordings with single-cell RNA-seq data identifies neuronal subtypes. Nat Biotech. 34:175–183.

Garabedian CE, Jones SR, Merzenich MM, Dale A, Moore CI. 2003. Band-pass response properties of rat SI neurons. J Neurophysiol. 90:1379.

Garcia-Junco-Clemente P, Ikrar T, Tring E, Xu X, Ringach DL, Trachtenberg JT. 2017. An inhibitory pull-push circuit in frontal cortex. Nat Neurosci. 20(3):389–392.

Gentet LJ, Kremer Y, Taniguchi H, Huang ZJ, Staiger JF, Petersen CCH. 2012. Unique functional properties of somatostatin-expressing GABAergic neurons in mouse barrel cortex. Nat Neurosci. 15:607–612.

Gibson JR, Beierlein M, Connors BW. 1999. Two networks of electrically coupled inhibitory neurons in neocortex. Nature. 402:75–79.

Gonzalez-Burgos G, Cho RY, Lewis DA. 2015. Alterations in cortical network oscillations and parvalbumin neurons in schizophrenia. Biol Psychiatry. 77:1031–1040.

Gupta A, Wang Y, Markram H. 2000. Organizing principles for a diversity of GABAergic interneurons and synapses in the neocortex. Science. 287:273–278.

Hamilton DJ, Wheeler DW, White CM, Rees CL, Komendantov AO, Bergamino M, Ascoli GA. 2017. Name-calling in the hippocampus (and beyond): coming to terms with neuron types and properties. Brain Inform. 4:1–12.

Helmstaedter M, Feldmeyer D. 2010. Axons predict neuronal connectivity within and between cortical columns and serve as primary classifiers of interneurons in a cortical column. In: Feldmeyer D, Lübke JHR, editors. New aspects of axonal structure and function. Boston, MA: Springer US. p. 141–155.

Helmstaedter M, Sakmann B, Feldmeyer D. 2009a. L2/3 interneuron groups defined by multiparameter analysis of axonal projection, dendritic geometry, and electrical excitability. Cereb Cortex. 19:951–962.

Helmstaedter M, Sakmann B, Feldmeyer D. 2009b. Neuronal correlates of local, lateral, and translaminar inhibition with reference to cortical columns. Cereb Cortex. 19:926–937.

Helmstaedter M, Sakmann B, Feldmeyer D. 2009c. The relation between dendritic geometry, electrical excitability, and axonal projections of L2/3 interneurons in rat barrel cortex. Cereb Cortex. 19:938–950.

Jiang X, Lachance M, Rossignol E. 2016. Involvement of cortical fast-spiking parvalbumin-positive basket cells in epilepsy. Prog Brain Res. 226:81–126.

Jiang X, Shen S, Cadwell CR, Berens P, Sinz F, Ecker AS, Patel S, Tolias AS. 2015. Principles of connectivity among morphologically defined cell types in adult neocortex. Science. 350: aac9462.

Johnson MB, Walsh CA. 2017. Cerebral cortical neuron diversity and development at single-cell resolution. Curr Opin Neurobiol. 42:9–16.

Jones HE, Grieve KL, Wang W, Sillito AM. 2001. Surround suppression in primate V1. J Neurophysiol. 86:2011–2028.

Kalanithi PS, Zheng W, Kataoka Y, DiFiglia M, Grantz H, Saper CB, Schwartz ML, Leckman JF, Vaccarino FM. 2005. Altered parvalbumin-positive neuron distribution in basal ganglia of individuals with Tourette syndrome. Proc Natl Acad Sci USA. 102:13307–13312.

Karagiannis A, Gallopin T, David C, Battaglia D, Geoffroy H, Rossier J, Hillman EM, Staiger JF, Cauli B. 2009. Classification of NPY-expressing neocortical interneurons. J Neurosci. 29: 3642–3659.

Karnani MM, Jackson J, Ayzenshtat I, Sichani AH, Manoocheri K, Kim S, Yuste R. 2016. Opening holes in the blanket of inhibition: localized lateral disinhibition by VIP interneurons. J Neurosci. 36:3471–3480.

Kato HK, Asinof SK, Isaacson JS. 2017. Network-level control of frequency tuning in auditory cortex. Neuron. 95:412–423.e4.

Kepecs A, Fishell G. 2014. Interneuron cell types are fit to function. Nature. 505:318–326.

Klausberger T, Somogyi P. 2008. Neuronal diversity and temporal dynamics: the unity of hippocampal circuit operations. Science. 321:53–57.

Koelbl C, Helmstaedter M, Lübke J, Feldmeyer D. 2015. A barrel-related interneuron in layer 4 of rat somatosensory cortex with a high intrabarrel connectivity. Cereb Cortex. 25: 713–725.

Kolomiets B, Marzo A, Caboche J, Vanhoutte P, Otani S. 2009. Background dopamine concentration dependently facilitates long-term potentiation in rat prefrontal cortex through postsynaptic activation of extracellular signal-regulated kinases. Cereb Cortex. 19:2708–2718.

Kubota Y, Shigematsu N, Karube F, Sekigawa A, Kato S, Yamaguchi N, Hirai Y, Morishima M, Kawaguchi Y. 2011. Selective coexpression of multiple chemical markers defines discrete populations of neocortical GABAergic neurons. Cereb Cortex. 21:1803–1817.

Laaris N, Keller A. 2002. Functional independence of layer IV barrels. J Neurophysiol. 87:1028–1034.

Lake BB, Ai R, Kaeser GE, Salathia NS, Yung YC, Liu R, Wildberg A, Gao D, Fung H-L, Chen S. 2016. Neuronal subtypes and diversity revealed by single-nucleus RNA sequencing of the human brain. Science. 352:1586–1590.

Land PW, Kandler K. 2002. Somatotopic organization of rat thalamocortical slices. J Neurosci Methods. 119:15–21.

Larkum M. 2013. A cellular mechanism for cortical associations: an organizing principle for the cerebral cortex. Trends Neurosci. 36:141–151.

Larkum ME, Kaiser KMM, Sakmann B. 1999. Calcium electrogenesis in distal apical dendrites of layer 5 pyramidal cells at a critical frequency of back-propagating action potentials. Proc Natl Acad Sci USA. 96:14600–14604.

Larkum ME, Zhu JJ. 2002. Signaling of layer 1 and whisker-evoked Ca2+ and Na+ action potentials in distal and terminal dendrites of rat neocortical pyramidal neurons in vitro and in vivo. J Neurosci. 22:6991–7005.

Lee S, Hjerling-Leffler J, Zagha E, Fishell G, Rudy B. 2010. The largest group of superficial neocortical GABAergic interneurons expresses ionotropic serotonin receptors. J Neurosci. 30: 16796–16808.

Lerner TN, Ye L, Deisseroth K. 2016. Communication in neural circuits: tools, opportunities, and challenges. Cell. 164: 1136–1150.

Li L-y, Ji X-Y, Liang F, Li Y-T, Xiao Z, Tao HW, Zhang LI. 2014. A feedforward inhibitory circuit mediates lateral refinement of sensory representation in upper layer 2/3 of mouse primary auditory cortex. J Neurosci. 34:13670–13683.

Lubke J, Roth A, Feldmeyer D, Sakmann B. 2003. Morphometric analysis of the columnar innervation domain of neurons connecting layer 4 and layer 2/3 of juvenile rat barrel cortex. Cereb Cortex. 13:1051–1063.

Ma Y, Hu H, Berrebi AS, Mathers PH, Agmon A. 2006a. Distinct subtypes of somatostatin-containing neocortical interneurons revealed in transgenic mice. J Neurosci. 26:5069–5082.

Ma Y, Hu H, Berrebi AS, Mathers PH, Agmon A. 2006b. Distinct subtypes of somatostatin-containing neocortical interneurons revealed in transgenic mice. J Neurosci. 26:5069–5082.

MacQueen J. Some methods for classification and analysis of multivariate observations. 1967: Oakland, CA, USA. p. 281–297.

Major G, Larkum ME, Schiller J. 2013. Active properties of neocortical pyramidal neuron dendrites. Annu Rev Neurosci. 36: 1–24.

Markram H, Toledo-Rodriguez M, Wang Y, Gupta A, Silberberg G, Wu C. 2004. Interneurons of the neocortical inhibitory system. Nat Rev Neurosci. 5:793–807.

Marx M, Gunter RH, Hucko W, Radnikow G, Feldmeyer D. 2012. Improved biocytin labeling and neuronal 3D reconstruction. Nat Protoc. 7:394–407.

McBain CJ, Fisahn A. 2001. Interneurons unbound. Nat Rev Neurosci. 2:11–23.

McGarry LM, Packer AM, Fino E, Nikolenko V, Sippy T, Yuste R. 2010. Quantitative classification of somatostatin-positive neocortical interneurons identifies three interneuron subtypes. Front Neural Circuits. 4:12.

Meyer HS, Schwarz D, Wimmer VC, Schmitt AC, Kerr JN, Sakmann B, Helmstaedter M. 2011. Inhibitory interneurons in a cortical column form hot zones of inhibition in layers 2 and 5A. Proc Natl Acad Sci USA. 108:16807–16812.

Miller MN, Okaty BW, Nelson SB. 2008. Region-specific spike-frequency acceleration in layer 5 pyramidal neurons mediated by Kv1 subunits. J Neurosci. 28:13716–13726.

Miyoshi G, Hjerling-Leffler J, Karayannis T, Sousa VH, Butt SJ, Battiste J, Johnson JE, Machold RP, Fishell G. 2010. Genetic fate mapping reveals that the caudal ganglionic eminence produces a large and diverse population of superficial cortical interneurons. J Neurosci. 30:1582–1594.

Miyoshi G, Young A, Petros T, Karayannis T, Chang MM, Lavado A, Iwano T, Nakajima M, Taniguchi H, Huang ZJ. 2015. Prox1 regulates the subtype-specific development of caudal ganglionic eminence-derived GABAergic cortical interneurons. J Neurosci. 35:12869–12889.

Muralidhar S, Wang Y, Markram H. 2013. Synaptic and cellular organization of layer 1 of the developing rat somatosensory cortex. Front Neuroanat. 7:52.

Muñoz W, Tremblay R, Levenstein D, Rudy B. 2017. Layer-specific modulation of neocortical dendritic inhibition during active wakefulness. Science. 355:954–959.

Narayanan RT, Egger R, Johnson AS, Mansvelder HD, Sakmann B, de Kock CPJ, Oberlaender M. 2015. Beyond columnar organization: cell type- and target layer-specific principles of horizontal axon projection patterns in rat vibrissal cortex. Cerebral Cortex. 25:4450–4468.

Oláh S, Komlósi G, Szabadics J, Varga C, Tóth É, Barzó P, Tamás G. 2007. Output of neurogliaform cells to various neuron types in the human and rat cerebral cortex. Front Neural Circuits. 1:4.

Overstreet-Wadiche L, McBain CJ. 2015. Neurogliaform cells in cortical circuits. Nat Rev Neurosci. 16:458–468.

Parra P, Gulyas AI, Miles R. 1998. How many subtypes of inhibitory cells in the hippocampus? Neuron. 20:983–993.

Paul A, Crow M, Raudales R, He M, Gillis J, Huang ZJ. 2017. Transcriptional architecture of synaptic communication delineates GABAergic neuron identity. Cell. 171:522–539 e20.

Pellegri G, Magistretti PJ, Martin JL. 1998. VIP and PACAP potentiate the action of glutamate on BDNF expression in mouse cortical neurones. Eur J Neurosci. 10:272–280.

Petersen CC, Sakmann B. 2001. Functionally independent columns of rat somatosensory barrel cortex revealed with voltage-sensitive dye imaging. J Neurosci. 21:8435–8446.

Porter JT, Cauli B, Staiger JF, Lambolez B, Rossier J, Audinat E. 1998. Properties of bipolar VIPergic interneurons and their excitation by pyramidal neurons in the rat neocortex. Eur J Neurosci. 10:3617–3628.

Porter JT, Johnson CK, Agmon A. 2001. Diverse types of interneurons generate thalamus-evoked feedforward inhibition in the mouse barrel cortex. J Neurosci. 21:2699–2710.

Pronneke A, Scheuer B, Wagener RJ, Mock M, Witte M, Staiger JF. 2015. Characterizing VIP neurons in the barrel cortex of VIPcre/tdTomato mice reveals layer-specific differences. Cereb Cortex. 25:4854–4868.

Qi G, van Aerde K, Abel T, Feldmeyer D. 2017. Adenosine differentially modulates synaptic transmission of excitatory and inhibitory microcircuits in layer 4 of rat barrel cortex. Cereb Cortex. 27:4411–4422.

Radnikow G, Günter RH, Marx M, Feldmeyer D. 2012. Morpho-functional mapping of cortical networks in brain slice preparations using paired electrophysiological recordings. In: Fellin T, Halassa MM, editors. Neuronal network analysis: concepts and experimental approaches. Totowa, NJ, USA: Humana Press. p. 405–431.

Rees CL, Moradi K, Ascoli GA. 2017. Weighing the evidence in Peters' rule: does neuronal morphology predict connectivity? Trends Neurosci. 40:63–71.

Rousseeuw PJ. 1987. Silhouettes: a graphical aid to the interpretation and validation of cluster analysis. J Comput Appl Math. 20:53–65.

Rozov A, Jerecic J, Sakmann B, Burnashev N. 2001. AMPA receptor channels with long-lasting desensitization in bipolar interneurons contribute to synaptic depression in a novel feedback circuit in layer 2/3 of rat neocortex. J Neurosci. 21:8062.

Rubin AN, Kessaris N. 2013. PROX1: a lineage tracer for cortical interneurons originating in the lateral/caudal ganglionic eminence and preoptic area. PLoS ONE. 8:e77339.

Rudy B, Fishell G, Lee S, Hjerling-Leffler J. 2011. Three groups of interneurons account for nearly 100% of neocortical GABAergic neurons. Dev Neurobiol. 71:45–61.

Sachdev RN, Krause MR, Mazer JA. 2012. Surround suppression and sparse coding in visual and barrel cortices. Front Neural Circuits. 6:43.

Santana R, McGarry L, Bielza C, Larrañaga P, Yuste R. 2013. Classification of neocortical interneurons using affinity propagation. Front Neural Circuits. 7:185.

Smith MA. 2006. Surround suppression in the early visual system. J Neurosci. 26:3624–3625.

Stuart GJ, Dodt HU, Sakmann B. 1993. Patch-clamp recordings from the soma and dendrites of neurons in brain slices using infrared video microscopy. Pflügers Archiv. 423:511–518.

Sun QQ, Huguenard JR, Prince DA. 2006. Barrel cortex microcircuits: thalamocortical feedforward inhibition in spiny stellate cells is mediated by a small number of fast-spiking interneurons. J Neurosci. 26:1219–1230.

Tabuchi K, Blundell J, Etherton MR, Hammer RE, Liu X, Powell CM, Sudhof TC. 2007. A neuroligin-3 mutation implicated in autism increases inhibitory synaptic transmission in mice. Science. 318:71–76.

Tamás G, Lőrincz A, Simon A, Szabadics A. 2003. Identified sources and targets of slow inhibition in the neocortex. Science. 299:1902–1905.

Tasic B, Menon V, Nguyen TN, Kim TK, Jarsky T, Yao Z, Levi B, Gray LT, Sorensen SA, Dolbeare T, et al. 2016. Adult mouse cortical cell taxonomy revealed by single cell transcriptomics. Nat Neurosci. 19:335–346.

Tremblay R, Lee S, Rudy B. 2016. GABAergic Interneurons in the neocortex: from cellular properties to circuits. Neuron. 91:260–292.

Uematsu M, Hirai Y, Karube F, Ebihara S, Kato M, Abe K, Obata K, Yoshida S, Hirabayashi M, Yanagawa Y, et al. 2008. Quantitative chemical composition of cortical GABAergic neurons revealed in transgenic venus-expressing rats. Cereb Cortex. 18:315–330.

Vucurovic K, Gallopin T, Ferezou I, Rancillac A, Chameau P, van Hooft JA, Geoffroy H, Monyer H, Rossier J, Vitalis T. 2010. Serotonin 3A receptor subtype as an early and protracted marker of cortical interneuron subpopulations. Cereb Cortex. 20:2333–2347.

Walker F, Möck M, Feyerabend M, Guy J, Wagener RJ, Schubert D, Staiger JF, Witte MD. 2016. Parvalbumin-and vasoactive

intestinal polypeptide-expressing neocortical interneurons impose differential inhibition on Martinotti cells. Nat Commun. 7:13664. doi:10.1038/ncomms13664.

Ward JH Jr. 1963. Hierarchical grouping to optimize an objective function. J Am Stat Assoc. 58:236–244.

Woolsey TA, van der Loos H. 1970. The structural organization of layer IV in the somatosensory region (SI) of mouse cerebral cortex. The description of a cortical field composed of discrete cytoarchitectonic units. Brain Res. 17:205–242.

Wozny C, Williams SR. 2011. Specificity of synaptic connectivity between layer 1 inhibitory interneurons and layer 2/3 pyramidal neurons in the rat neocortex. Cereb Cortex. 21: 1818–1826.

Xu H, Jeong HY, Tremblay R, Rudy B. 2013. Neocortical somatostatin-expressing GABAergic interneurons disinhibit the thalamorecipient layer 4. Neuron. 77:155–167.

Zeisel A, Munoz-Manchado AB, Codeluppi S, Lonnerberg P, La Manno G, Jureus A, Marques S, Munguba H, He L, Betsholtz C, et al. 2015. Brain structure. Cell types in the mouse cortex and hippocampus revealed by single-cell RNA-seq. Science. 347:1138–1142.

Zeng H, Sanes JR. 2017. Neuronal cell-type classification: challenges, opportunities and the path forward. Nat Rev Neurosci. 18:530–546.

Zhou X, Rickmann M, Hafner G, Staiger JF. 2017. Subcellular targeting of VIP boutons in mouse barrel cortex is layer-dependent and not restricted to interneurons. Cereb Cortex. 27(11):5353–5368.

Zhu Y, Zhu JJ. 2004. Rapid arrival and integration of ascending sensory information in layer 1 nonpyramidal neurons and tuft dendrites of layer 5 pyramidal neurons of the neocortex. J Neurosci. 24:1272–1279.